



Targeting the perivascular niche sensitizes disseminated tumour cells to chemotherapy

Patrick Carlson^{1,11}, Arko Dasgupta^{1,11}, Candice A. Grzelak^{1,11}, Jeanna Kim ^{1,11}, Alexander Barrett², Ilsa M. Coleman^{3,4}, Ryann E. Shor¹, Erica T. Goddard¹, Jinxiang Dai¹, Emma M. Schweitzer¹, Andrea R. Lim^{1,5}, Sarah B. Crist^{1,5}, David A. Cheresch^{6,7}, Peter S. Nelson^{3,4,8,9,10}, Kirk C. Hansen² and Cyrus M. Ghajar ^{1,3*}

The presence of disseminated tumour cells (DTCs) in bone marrow is predictive of poor metastasis-free survival of patients with breast cancer with localized disease. DTCs persist in distant tissues despite systemic administration of adjuvant chemotherapy. Many assume that this is because the majority of DTCs are quiescent. Here, we challenge this notion and provide evidence that the microenvironment of DTCs protects them from chemotherapy, independent of cell cycle status. We show that chemoresistant DTCs occupy the perivascular niche (PVN) of distant tissues, where they are protected from therapy by vascular endothelium. Inhibiting integrin-mediated interactions between DTCs and the PVN, driven partly by endothelial-derived von Willebrand factor and vascular cell adhesion molecule 1, sensitizes DTCs to chemotherapy. Importantly, chemosensitization is achieved without inducing DTC proliferation or exacerbating chemotherapy-associated toxicities, and ultimately results in prevention of bone metastasis. This suggests that prefacing adjuvant therapy with integrin inhibitors is a viable clinical strategy to eradicate DTCs and prevent metastasis.

Despite chemotherapeutic regimens and endocrine therapies that substantially improve patient survival, late, distant recurrence of breast cancer remains a problem. Nearly 10% of all patients with invasive breast carcinoma¹ and up to 17% of patients with oestrogen receptor positive (ER⁺) disease² relapse 5 years or more after adjuvant treatment. Cells that disseminate from the primary tumour before its detection and persist at distant sites despite systemic therapy are thought to be the source of these distant recurrences^{3–7}. Indeed, elimination of DTCs enhances metastasis-free survival of patients with breast cancer⁸, motivating a targeted and selective approach to eradicate DTCs before they emerge.

Currently, no such therapy exists. Instead, patients with invasive breast cancer are treated with regimens that include dose-dense Adriamycin (also known as doxorubicin) plus cyclophosphamide (AC) and/or paclitaxel (also known as Taxol)⁹. Non-proportional statistical modelling of patient survival shows that such regimens do not prevent late recurrence¹⁰, implying that chemotherapies do not effectively eradicate DTCs with metastasis-initiating potential. This assertion has been confirmed in clinical specimens^{3,5,11}, for which the continued presence of DTCs is associated with poor metastasis-free survival^{12,13}, and in animal models¹⁴, in which single DTCs persist despite application of cytotoxic therapy.

It is commonly assumed that DTCs resist chemotherapy because the vast majority are quiescent (that is, Ki67⁻)¹⁵. This assumption ignores a growing body of literature showing that the microenvironment mediates the resistance of solid primary tumours and of haematopoietic malignancies^{16–21}. In particular, a number of recent

studies have identified factors deposited within the PVN that protect tumour cells from radiotherapy²² and chemotherapy^{17,18}. In light of our prior demonstration that quiescent disseminated breast tumour cells reside within the PVN²³, we hypothesized that this niche may also confer resistance to therapy. We posited that if this was the case, and if the mechanisms underlying therapeutic resistance were distinct from those that regulate quiescence, it would open the door for new strategies to prevent metastasis⁴.

Here, we provide experimental support for this hypothesis. Namely, we show that chemoresistant DTCs associate with the PVN, where they are protected from chemotherapy by vascular endothelium, irrespective of their cell cycle status. Furthermore, we show that inhibiting key integrin-mediated interactions between DTCs and the PVN sensitizes DTCs to chemotherapy, and results in metastasis prevention. Importantly, chemosensitization is achieved without inducing quiescent DTCs to enter the cell cycle and without exacerbating chemotherapy-associated toxicities. These data suggest that prefacing adjuvant therapy with integrin inhibitors is a viable strategy to eradicate DTCs and prevent metastasis.

Results

Chemotherapy selects for perivascular DTCs. To determine whether DTCs that persist beyond the application of dose-dense chemotherapy occupy a specific niche, we implanted 4T07 cells expressing firefly luciferase and enhanced green fluorescent protein (ffluc-eGFP) into syngeneic (Balb/c) mice, and treated these mice after primary tumour resection with dose-dense AC or paclitaxel

¹Public Health Sciences Division/Translational Research Program, Fred Hutchinson Cancer Research Center, Seattle, WA, USA. ²Department of Biochemistry and Molecular Genetics, University of Colorado Anschutz Medical Campus, Aurora, CO, USA. ³Human Biology Division, Fred Hutchinson Cancer Research Center, Seattle, WA, USA. ⁴Clinical Research Division, Fred Hutchinson Cancer Research Center, Seattle, WA, USA. ⁵Graduate Program in Molecular and Cellular Biology, University of Washington, Seattle, WA, USA. ⁶Department of Pathology, University of California, San Diego, La Jolla, CA, USA. ⁷Sanford Consortium for Regenerative Medicine, La Jolla, CA, USA. ⁸Department of Medicine, University of Washington, Seattle, WA, USA. ⁹Department of Urology, University of Washington, Seattle, WA, USA. ¹⁰Department of Pathology, University of Washington, Seattle, WA, USA. ¹¹These authors contributed equally: Patrick Carlson, Arko Dasgupta, Candice A. Grzelak, Jeanna Kim. *e-mail: cghajar@fredhutch.org

for 5 weeks. We scaled down human dosing⁹ to account for the differences in body surface area between a human and a mouse²⁴ (Fig. 1a). Femurs from treated mice were stained, whole-mounted and imaged to readily identify eGFP⁺ tumour cells (Fig. 1b), quantify their number (Fig. 1c) and measure their distance to sites of interest (Fig. 1d–k). Given that both DTCs and haematopoietic stem cells are characterized by long-term quiescence and therapeutic resistance^{25,26}, we measured the distance from eGFP⁺ DTCs to the following three major niches shown to harbour haematopoietic stem cells: osteoblastic²⁷, megakaryocytic²⁸ and perivascular^{29–33}. An analysis of 350 DTCs revealed that DTCs were concentrated in the PVN of bone marrow (BM) following AC treatment (Fig. 1d,e); the average distance to the nearest blood vessel was 7.13 μm (Fig. 1f). Such an intimate localization was not observed with megakaryocytes or osteoblasts; on average, DTCs were 68.8 μm and 198 μm , respectively, apart from these cell types (Fig. 1g,h). Similar data were obtained following treatment with dose-dense paclitaxel (Fig. 1f–h). A comparison to vehicle-treated animals revealed that the average distance of DTCs to the vasculature decreased by 28.1% in mice treated with the AC regimen, whereas the average distance to the osteoblastic niche increased. Given the substantial reduction in DTC number observed in mice treated with AC (Fig. 1c), these data suggest that DTCs localized on vasculature, away from the BM–bone interface, are resistant to AC (Fig. 1f–h). An analysis of DTCs residing directly on vasculature confirmed this assertion. AC- and paclitaxel-based regimens doubled the percentage of DTCs residing on BM vasculature (Fig. 1i). Neither enriched for DTCs neighbouring megakaryocytes or osteoblasts (Fig. 1j,k).

To ensure that the effect observed was not specific to femurs, we performed cytometry on DTCs harboured within tibia of the same mice (Supplementary Fig. 1a,b). Here, AC treatment caused a 45.7% reduction in the average distance of DTCs to the BM vasculature (Supplementary Fig. 1c). Selection for DTCs residing directly on the vascular basement membrane was a contributor, as the percentage of DTCs occupying this compartment increased by 1.22-fold (Supplementary Fig. 1f). Conversely, the spatial relationship between DTCs and megakaryocytic or osteoblastic niches was essentially unchanged (Supplementary Fig. 1d,e,g,h).

Organotypic culture reveals that microvascular endothelium protects breast tumour cells from chemotherapy. Endothelial-derived (that is, angiocrine³⁴) factors regulate a host of biological processes spanning development and disorder³⁴. Previously, we developed organotypic models of the microvasculature of BM, called BM microvascular niches (MVNs), to study whether localization of dormant DTCs to the PVN reflected a functional consequence of DTC–endothelial cell interactions²³. Here, we applied these same models to determine whether endothelial cells protect breast tumour cells from chemotherapy. BM mesenchymal stem cells (MSCs) and BM MVNs were seeded sparsely with breast tumour cells to approach the scarcity of DTCs in BM^{35,36}. Of note, the MSCs did not drift towards an osteogenic or adipogenic phenotype over the course of these experiments (Supplementary Fig. 2). After 12 additional days, the BM MSC and MVN cultures were treated with increasing doses of doxorubicin or paclitaxel, and the DTC burden was analysed 5 days later (Fig. 2a). Basal HMT-3522-T4-2 (T4-2) breast tumour cells exhibited a dose-dependent response to doxorubicin (Fig. 2b) and paclitaxel (Fig. 2h) on BM stroma. In contrast, neither doxorubicin (Fig. 2c) nor paclitaxel (Fig. 2i) significantly reduced the DTC burden on BM MVNs at any dose tested. The disparity observed in DTC response between these two niches stemmed from a lack of DTC death in MVNs. Whereas doxorubicin induced DTC apoptosis by up to 59.0% on BM stroma (Fig. 2d,e), DTC death in BM MVNs increased by only 5.45% between vehicle and the highest dose of doxorubicin tested (2,500 nM; Fig. 2f,g). Response to paclitaxel was similar, topping out

at a rate of cell killing on MVNs (20.5%) that was only one-third the rate observed on BM stroma (Fig. 2j–m). Five-fluorouracil, a chemotherapeutic commonly used as an adjuvant in breast cancer treatment³⁷, and lapatinib, an epidermal growth factor (EGF) receptor-targeted therapy³⁸, also yielded dose-dependent responses on BM stroma that were obviated on MVNs (Supplementary Fig. 3a–h). MVN-mediated protection from doxorubicin-induced cell death was also observed with a luminal ER⁺ breast tumour cell line (MCF-7) (Supplementary Fig. 3i–l). Combined with our observations with murine BM (Fig. 1), these data demonstrate that the PVN promotes chemotherapeutic resistance of DTCs, and that endothelium is the principal cellular component of the PVN protecting DTCs from chemotherapy. However, these data do not delineate whether this effect is due simply to growth restraints imposed on DTCs by the PVN²³ or because of unique chemoprotective factors supplied by the endothelium.

Cell cycle status and therapeutic resistance are decoupled in the PVN. To look for evidence of a niche-specific, cell cycle-independent response to chemotherapy, we used three independent approaches. First, we examined only single DTCs that persisted on BM stroma or BM MVNs over the course of 17 days after application of the highest dose of doxorubicin (Fig. 3a) or paclitaxel (Fig. 3b). In each case, death of even single, ostensibly nonproliferative DTCs was reduced by half on MVNs (Fig. 3a,b).

Second, we engineered T4-2 cells to simultaneously express tdTomato and a mutant reporter of p27 (mVenus-p27K⁻), which delineates quiescent cells³⁹. tdTomato–mVenus-p27K⁻ T4-2 cells were seeded on BM stroma or MVNs and treated simultaneously after 12 days with 2,500 nM doxorubicin and a DEVD substrate (NucView405) that fluoresces following caspase-3-mediated cleavage⁴⁰. This approach allowed us to monitor in real-time DTC apoptosis on BM stroma and MVNs as a function of cell cycle status (Fig. 3c). In both niches, there was clear evidence of p27⁺ and p27⁻ tumour cells undergoing apoptosis in response to doxorubicin (Fig. 3d; Supplementary Videos 1–3). As expected, substantially fewer events were observed on BM MVNs than on BM stroma (Fig. 3d,e). However, the distribution of affected populations skewed in a manner that suggested MVNs protect tumour cells from apoptosis irrespective of their proliferation status (Fig. 3e). Namely, apoptosis on BM stroma occurred predominantly in p27⁻ tumour cells, whereas death on MVNs occurred evenly between p27⁺ and p27⁻ populations (Fig. 3e). This result suggests that stimulating tumour cell proliferation on MVNs would not sensitize tumour cells to apoptosis. We developed an approach to test this directly.

Our prior work implicated insulin-like growth factor (IGF) binding proteins as negative regulators of breast tumour cell outgrowth²³, suggesting that IGF1 supplementation would stimulate proliferation of quiescent breast tumour cells on MVNs. Administration of IGF1 after 10 days of co-culture (Supplementary Fig. 4a) stimulated the proliferation of quiescent DTCs, judged by a threefold increase in DTC outgrowth (Supplementary Fig. 4b), and a nearly fivefold increase in Ki67⁺ cells (Supplementary Fig. 4c). However, priming co-cultures with IGF1 before treatment with doxorubicin (Fig. 3f) did not sensitize re-emerging tumour cells to chemotherapy (Fig. 3g,h). Thus, all three lines of evidence presented here suggest that perivascular DTCs resist chemotherapy not because they are quiescent but because components within the PVN protect them from chemotherapy. Therefore, identifying and interfering with this signalling became our priority.

Integrin-mediated interactions between DTCs and microvascular endothelium protect DTCs from chemotherapy. To identify putative, endothelial-derived factors that protect DTCs from chemotherapy, we sequenced the whole transcriptome of BM stroma and BM MVNs by RNA sequencing (RNA-seq). A pathway analysis

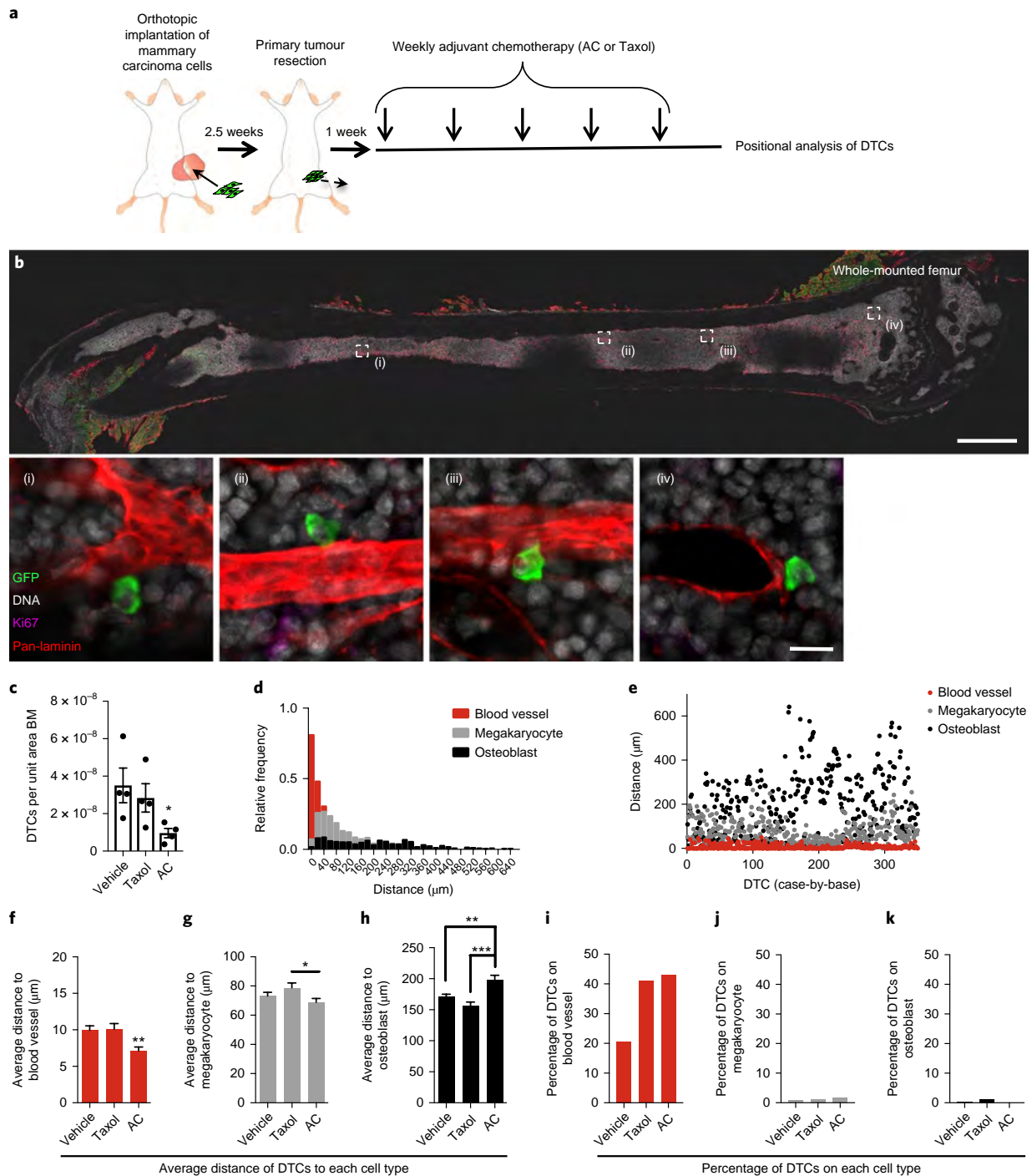


Fig. 1 | Dose-dense chemotherapeutic regimens select for perivascular disseminated tumour cells. a, Schematic of the experiment to identify whether DTCs localize to a specific niche following dose-dense chemotherapy. After resection of the fluc-eGFP⁺ primary tumour, mice were treated with five cycles of weekly AC (2 mg per kg of Adriamycin and 60 mg per kg of cyclophosphamide), Taxol (20 mg per kg) or vehicle. DTC position within BM was analysed by staining and whole-mounting femurs 1 week after the final treatment. **b**, Top: tile scans encompassing the entire exposed face of the BM and the full Z-depth (~100 μm) that could be imaged using this method were acquired. Bottom: four examples (corresponding to (i)–(iv) from the top image) of perivascular, GFP⁺, Ki67⁺ DTCs are shown in BM following AC treatment. Scale bar, 1 mm (top), 20 μm (bottom). **c**, Quantification of DTCs in femoral BM of vehicle-, Taxol- and AC-treated animals, normalized to BM area analysed and volume of the primary tumour at resection. For each treatment, $n=4$ femurs from 4 different animals were analysed. * $P=0.022$ compared with vehicle-treated mice by Kruskal–Wallis and Dunn’s test to correct for multiple comparisons. A total of 350 DTCs were analysed across $n=3$ femurs from 3 different animals. **d,e**, Results were binned in histogram format (**d**) or dot-plotted (**e**) as individual distances to the nearest blood vessel, megakaryocyte or osteoblast. **f–h**, The average of these distances to the nearest blood vessel (**f**), megakaryocyte (**g**) and osteoblast (**h**) for mice that underwent treatment with vehicle ($n=488$ DTCs analysed across 3 animals), AC ($n=350$) or Taxol ($n=327$). ** $P=0.0039$ (versus vehicle) or $P=0.0061$ (versus Taxol) for **f**, * $P=0.047$ for **g**, ** $P=0.0017$ and *** $P<0.0001$ for **h**, all by one-way ANOVA followed by Tukey’s multiple comparisons test. **i–k**, The percentage of DTCs quantified across three mice in direct contact with blood vessels (**i**), megakaryocytes (**j**) and osteoblasts (**k**) for mice that underwent treatment with vehicle, Taxol or AC. For **c, f–h**, the centre line represents the mean and error bars the s.e.m. Source data are provided in Supplementary Table 1.

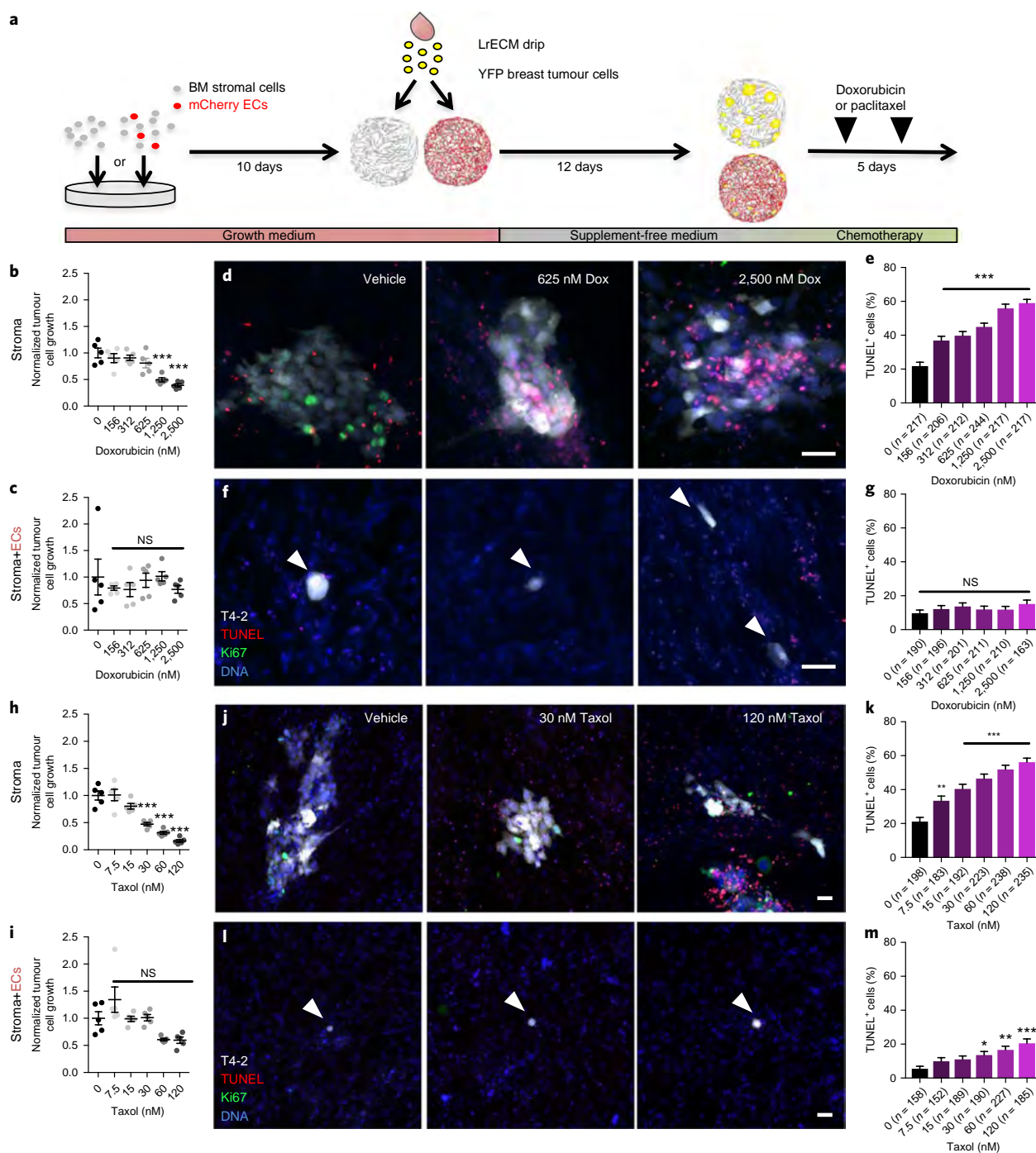


Fig. 2 | Microvascular endothelium protects breast tumour cells from chemotherapy. **a**, Schematic of experiment to determine whether endothelium protects DTCs from chemotherapy. **b,c**, Dose response of T4-2 breast cancer cells on BM stroma (**b**) and MVNs (stroma plus endothelial cells (ECs); **c**) to doxorubicin ($n=5$ independent experiments). NS, not significant, $***P < 0.0001$ compared to vehicle by one-way ANOVA and Dunnett's multiple comparison test. Following treatment, cultures were TUNEL stained to assess apoptosis. **d**, Representative images of TUNEL-stained T4-2 'DTCs' treated with increasing doses of doxorubicin (Dox) on BM stroma. **e**, Percentage of TUNEL⁺ DTCs per DTC cluster as a function of dose. $***P < 0.0001$ for all conditions versus vehicle by one-way ANOVA and Dunnett's multiple comparisons test. **f**, Representative images of TUNEL-stained T4-2 DTCs (white arrowheads) treated with increasing doses of Dox on BM MVNs. **g**, Percentage of TUNEL⁺ DTCs per DTC cluster as a function of dose. NS denotes no significance compared to vehicle by one-way ANOVA and Dunnett's multiple comparisons test. **h,i**, Dose response of T4-2 DTCs on BM stroma (**h**) and MVNs (**i**) to Taxol ($n=5$ independent experiments). $***P < 0.0001$ by one-way ANOVA and Dunnett's multiple comparison test compared to vehicle. **j**, Representative images of TUNEL-stained T4-2 cells treated with increasing doses of Taxol on BM stroma. **k**, Percentage of TUNEL-positive DTCs per DTC cluster as a function of dose. $***P < 0.0001$ compared to vehicle by one-way ANOVA and Dunnett's multiple comparisons test. **l**, Representative images of TUNEL-stained T4-2 cells (white arrowheads) treated with increasing doses of Taxol on BM MVNs. **m**, Percentage of TUNEL⁺ DTCs per DTC cluster as a function of dose. $*P = 0.0437$, $**P = 0.0012$, $***P < 0.0001$ compared to vehicle by one-way ANOVA and Dunnett's multiple comparisons test. For **d, f, j** and **l**, scale bars represent 50 μm . For **b, c, e, g-l, k, m**, the centre line represents the mean and error bars the s.e.m. For TUNEL analyses, the number of cells (predominantly single cells and clusters of 2-4 cells) analysed per condition across $n=3$ independent experiments is stated within each panel. Source data are provided in Supplementary Table 1.

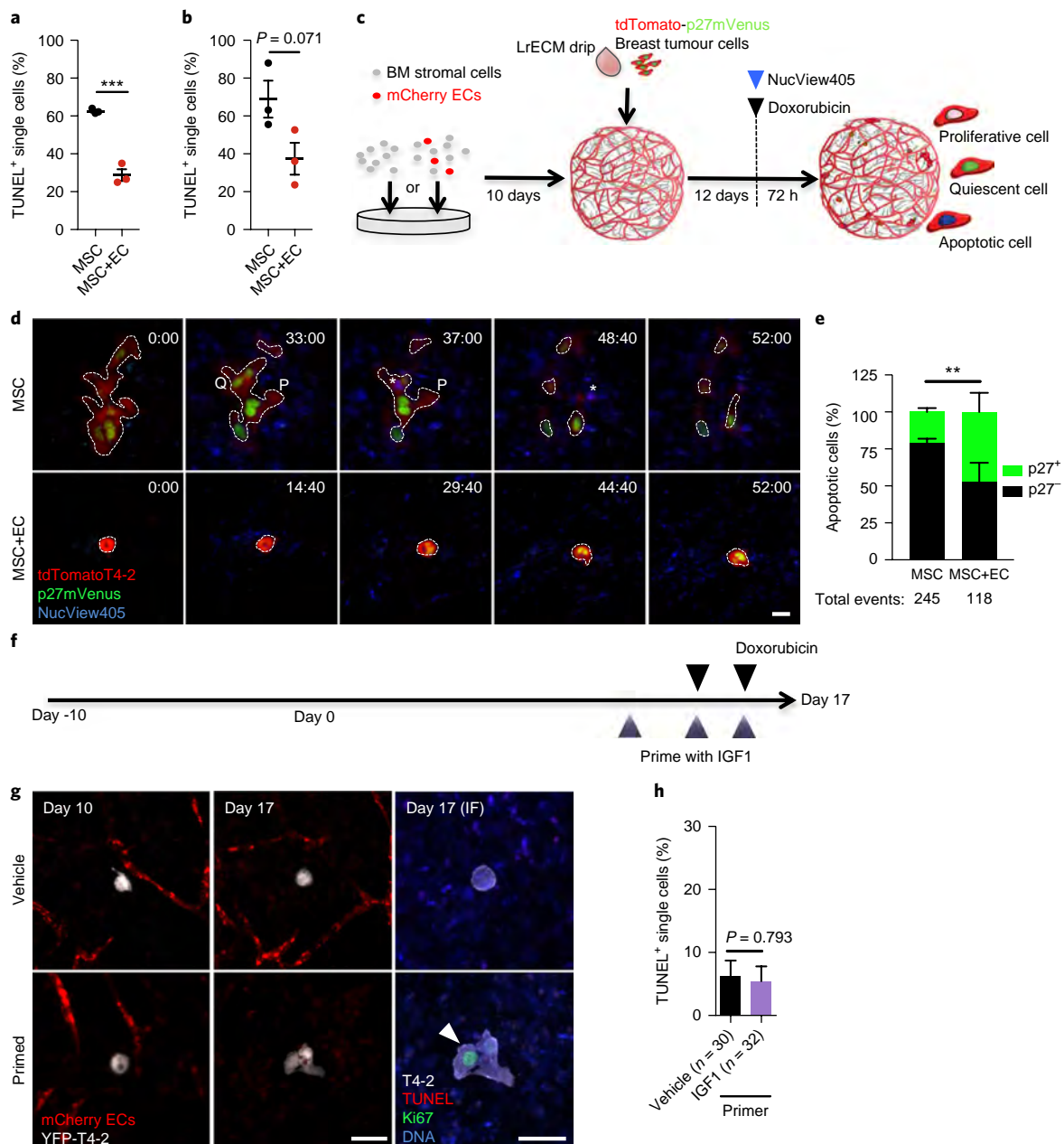


Fig. 3 | Perivascular niche-mediated chemoprotection does not depend on DTC cell cycle status. **a,b**, Analysis of single DTCs on stroma (MSC) or BM MVNs (MSC+ECs) following treatment with 2,500 nM doxorubicin (**a**) or 120 nM Taxol (**b**). Data depict the percentage of TUNEL⁺ single cells over $n = 3$ independent experiments. *** $P = 0.0004$ (**a**) and $P = 0.0713$ (**b**) by unpaired, two-tailed *t*-test. **c**, Schematic of the experiment to determine how cell cycle status influences the response to doxorubicin on BM stroma and BM MVNs. Here, cultures were seeded with T4-2 cells expressing tdTomato and a mVenus-p27K⁻ reporter, treated with 2,500 nM doxorubicin and NucView405 to label apoptotic cells, and imaged for 72 h. **d**, Stills from time-lapse videos on BM stroma (top) or BM MVNs (bottom). Time is indicated as hours:minutes. Q indicates a quiescent cell that subsequently undergoes apoptosis (white asterisk), and P denotes a proliferative cell that subsequently undergoes apoptosis (white asterisk), both on stroma. Scale bar, 20 μm . **e**, Quantification of relative percentages of p27⁺ and p27⁻ T4-2 cells that apoptose within 72 h of doxorubicin treatment on BM stroma and on BM MVNs from $n = 6$ independent videos per condition. ** $P = 0.0027$ comparing MSC to MSC+EC by two-way ANOVA. **f**, Schematic of the experiment to determine whether priming MVNs with IGF1 to trigger DTC proliferation sensitizes DTCs to doxorubicin. **g**, Representative images of quiescent, microvascular-associated DTCs at day 10 (left), and after priming with vehicle or with 300 ng ml⁻¹ IGF1 at day 17 (middle). Cultures were fixed and stained at this time point to analyse the proliferative status and viability of tumour cells (right). IF, immunofluorescence. White arrowheads denote Ki67-positive DTC after priming with IGF1. Scale bars, 50 μm . **h**, Percentage of TUNEL⁺ DTCs per DTC cluster as a function of priming with vehicle or 300 ng ml⁻¹ IGF1, and treating with 2,500 nM doxorubicin. $n = 30$ and 32 cells from single cells or clusters of mostly 2–4 cells were analysed for the vehicle- and IGF1-primed conditions, respectively, over $n = 3$ independent experiments. *P* value was calculated using unpaired, two-tailed *t*-test. For **a**, **b**, **e** and **h**, the centre line represents the mean and error bars the s.e.m. Source data are provided in Supplementary Table 1.

revealed that “integrin binding” constituted one of the most significantly enriched molecular functions in MVNs (Fig. 4a). A number of the most significantly enriched integrin–cell surface interaction

genes in this dataset (Fig. 4b,c) were confirmed by quantitative proteomic profiling of extracellular matrix (ECM) (Fig. 4d). This—along with a growing body of evidence linking therapeutic resistance to

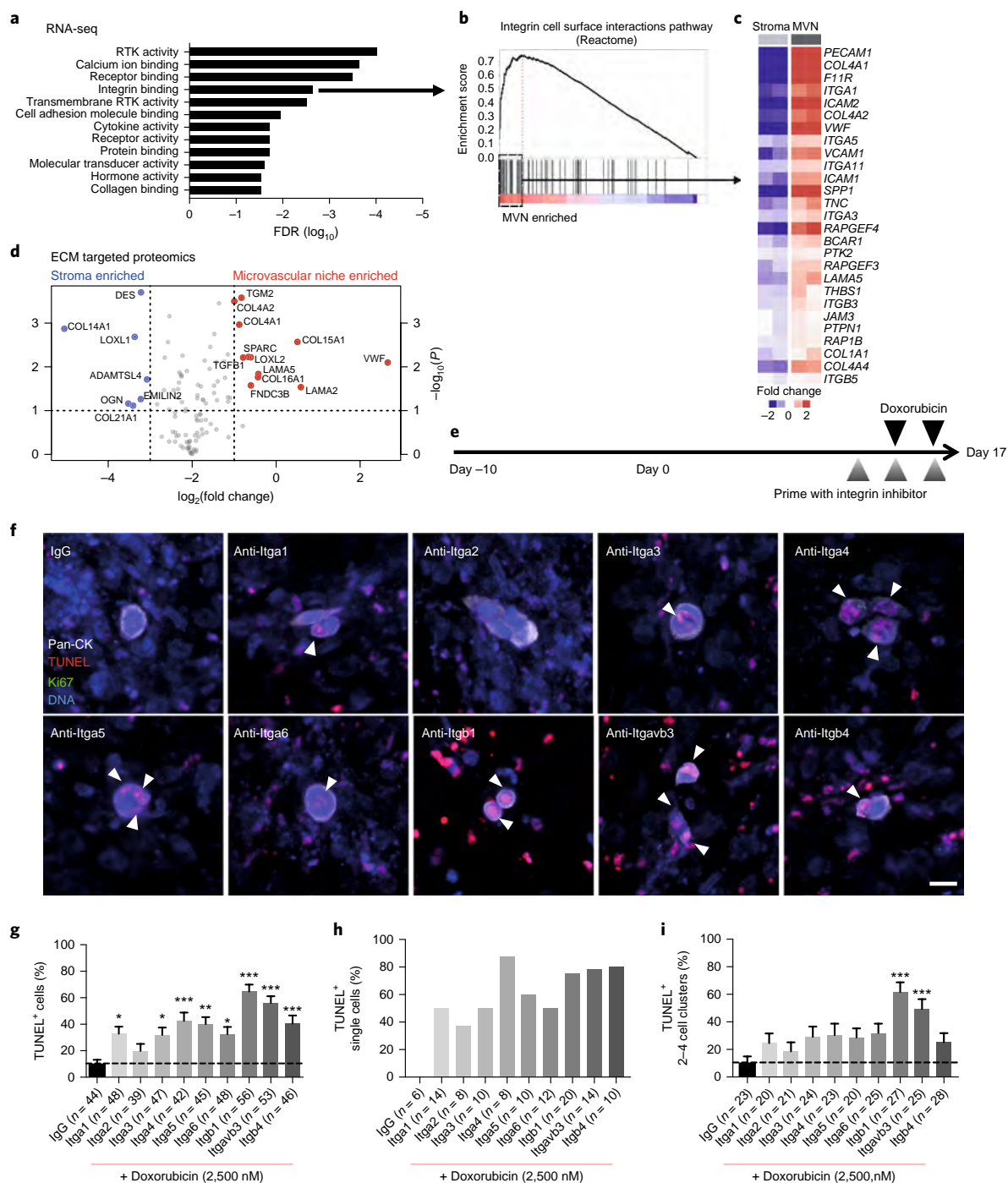


Fig. 4 | Integrin β , and integrin $\alpha_5\beta_3$ protect perivascular-disseminated tumour cells from chemotherapy. **a**, Functional enrichment analysis conducted on whole transcriptome sequencing data derived from BM stroma and BM MVNs ($n=2$ biologically independent samples; threefold differential expression cut-off). Enrichment was tested by Fisher's exact test and controlled for multiple testing by the FDR. FDR ($-\log_{10}$) of significantly enriched Gene Ontology molecular function terms are plotted. Integrin binding was among the most enriched molecular functions. **b**, GSEA of the Reactome "Integrin cell surface interactions" pathway. The leading edge subset of genes defining the enrichment are outlined. **c**, Heatmap of relative expression values in stroma and MVNs of the 27 target genes that define the leading edge GSEA analysis in **b**. **d**, Quantitative, ECM-targeted proteomic data displayed as a volcano plot, showing significantly enriched genes in BM stroma and BM MVNs. Data are derived from $n=3$ biologically independent samples; P values generated by unpaired, nonparametric, two-sided t -test (Mann-Whitney). **e**, Schematic of experiment to test whether priming DTCs with inhibitory antibodies targeting integrin subunits sensitizes DTCs to doxorubicin. **f**, Representative images of fixed and TUNEL-stained T4-2 DTCs on BM MVNs following treatment with the array of integrin function blocking antibodies listed (or isotype/IgG control) and 2,500 nM doxorubicin. White arrowheads denote apoptotic DTCs. Scale bar, 20 μm . **g-i**, Quantification of TUNEL⁺ DTCs and DTC clusters following treatment with the array of function blocking antibodies listed (or isotype/IgG control) and 2,500 nM doxorubicin on BM MVNs yielded the total percentage of TUNEL⁺ cells across 1-10 DTCs or DTC clusters (**g**), TUNEL⁺ single DTCs (**h**) and TUNEL⁺ DTCs within clusters of 2-4 DTCs (**i**). The number of cells or cell clusters analysed per condition is stated within each panel. For **g** and **i**, * $P < 0.05$, ** $P < 0.01$ and *** $P < 0.001$ when compared to control (IgG) by one-way ANOVA and Dunnett's multiple comparisons test. The centre line represents the mean and error bars the s.e.m. Source data are provided in Supplementary Table 1.

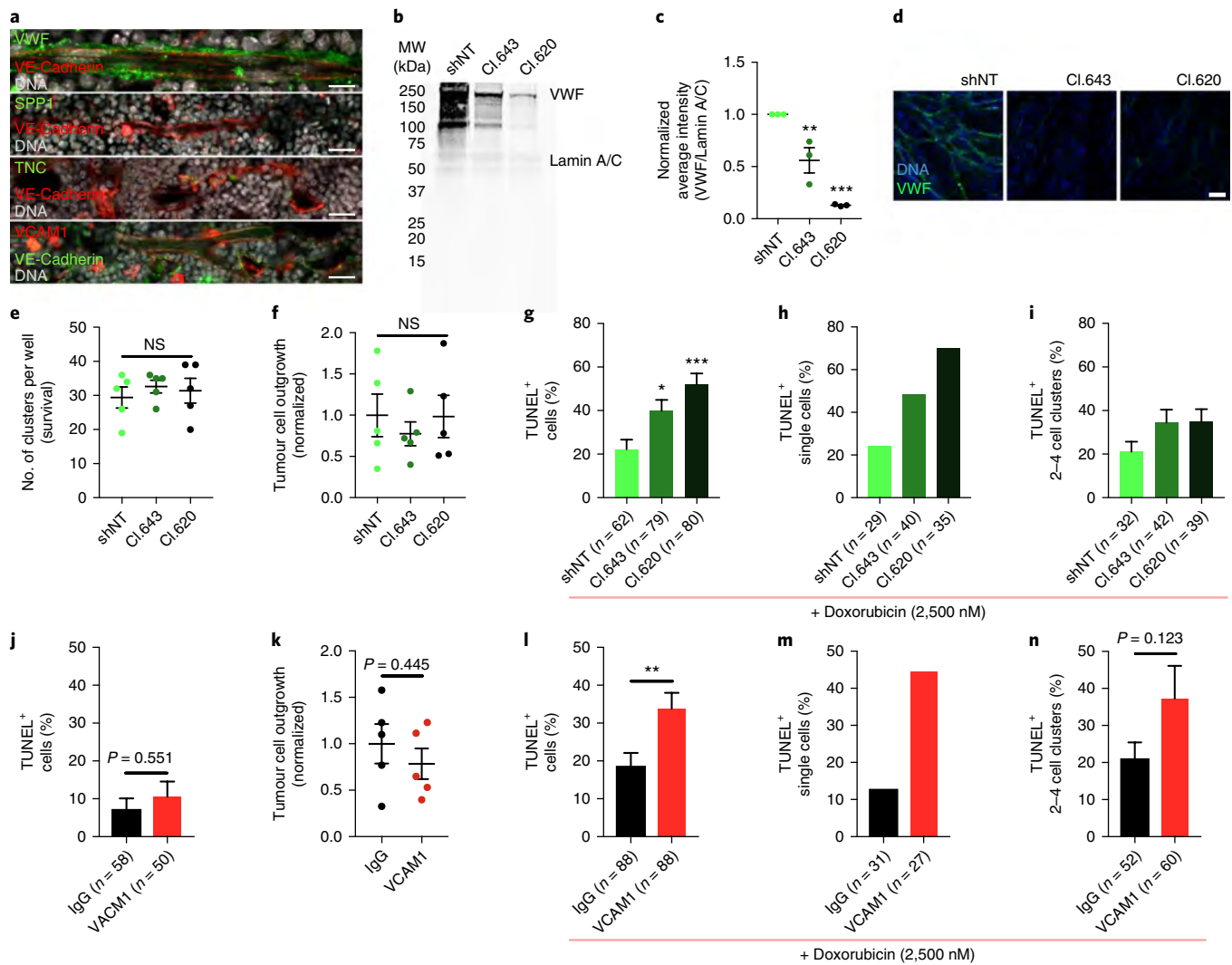


Fig. 5 | Endothelial VWF and VCAM1 confer DTC resistance to doxorubicin. **a**, Immunofluorescence staining for VWF, SPP1, TNC and VCAM1 to assess localization to BM microvessels. Scale bar, 20 μm (VWF), 10 μm (SPP1, TNC and VCAM1). **b**, Representative immunoblot of ECs infected with NT shRNA (shNT) or two different shRNA clones targeting VWF (Cl.643 and Cl.620). The blot was co-stained for VWF and the nuclear envelope proteins lamin A/C (loading control). **c**, Densitometry from $n=3$ biologically independent samples, normalized to the intensity of the shNT band on each blot. $**P=0.008$, $***P=0.0002$ by one-way ANOVA and Dunnett's multiple comparisons test. **d**, Representative immunostaining images ($n=3$ independent experiments) for VWF in BM MVNs composed of shNT ECs or shVWF ECs after 27 days in selection-free media. Scale bar, 100 μm . **e-f**, Number of clusters (**e**) and tumour cell outgrowth (**f**) ($n=5$ independent experiments) in the absence of doxorubicin ($n=5$ independent experiments). NS, no significance between shNT and shVWF conditions by one-way ANOVA and Dunnett's multiple comparisons test. **g-i**, Quantification of TUNEL⁺ DTCs (overall) (**g**), single DTCs (**h**) and 2-4 cell DTC clusters (**i**) following treatment with 2,500 nM doxorubicin as a function of endothelial VWF expression. In **g**, $*P=0.0266$ and $***P<0.0001$ versus shNT by one-way ANOVA and Dunnett's multiple comparisons test. **j-k**, TUNEL⁺ DTCs or DTC clusters (**j**) and tumour cell outgrowth (**k**) on BM MVNs following treatment with only VCAM1 blocking antibody or mouse IgG control ($n=5$ independent experiments). Stated P values calculated via unpaired, two-tailed t -test. **l-n**, The percentage of TUNEL⁺ DTCs (overall) (**l**), single DTCs (**m**) and clusters of 2-4 DTCs (**n**) from BM MVNs primed with VCAM1 function blocking antibody or isotype control before treatment with 2,500 nM doxorubicin (as in Fig. 4e). $**P=0.0054$ by unpaired, two-tailed t -test. For TUNEL analyses, the number of cells (predominantly single cells and clusters of 2-4 cells) analysed per condition across $n=3$ independent experiments is stated within each panel. For **c**, **e-g**, **l-j-l** and **n**, the centre line represents the mean and the error bars the s.e.m. Source data are provided in Supplementary Table 1.

integrin-mediated adhesion to ECM^{16,19,21,41,42}—led us to interrogate a series of integrin receptors that could mediate the protective interactions between DTCs and molecules within the PVN. We used an array of high-quality integrin-targeted function blocking antibodies to prime MVNs before doxorubicin treatment (Fig. 4e). Given the abundance of single DTCs and the typical size of DTC clusters reported in patient BM⁴³, we focused on single breast tumour cells and clusters of ≤ 10 cells. Priming with isotype control antibody did not sensitize

DTCs to apoptosis (compare Fig. 4f,g with Fig. 2f,g). Blocking the adhesion of a number of integrin subunits led to a substantial increase in sensitivity to doxorubicin (Fig. 4g-i). Antibodies targeting integrin β_1 (anti-Itgb1) and integrin $\alpha_3\beta_3$ (anti-Itgavb3) yielded the best response, killing 56.0–64.6% of cells overall (about a sixfold increase above baseline), and sensitizing up to 78.6% of single DTCs to doxorubicin (Fig. 4h). Furthermore, these antibodies were the only two to markedly sensitize DTC clusters to doxorubicin (Fig. 4i).

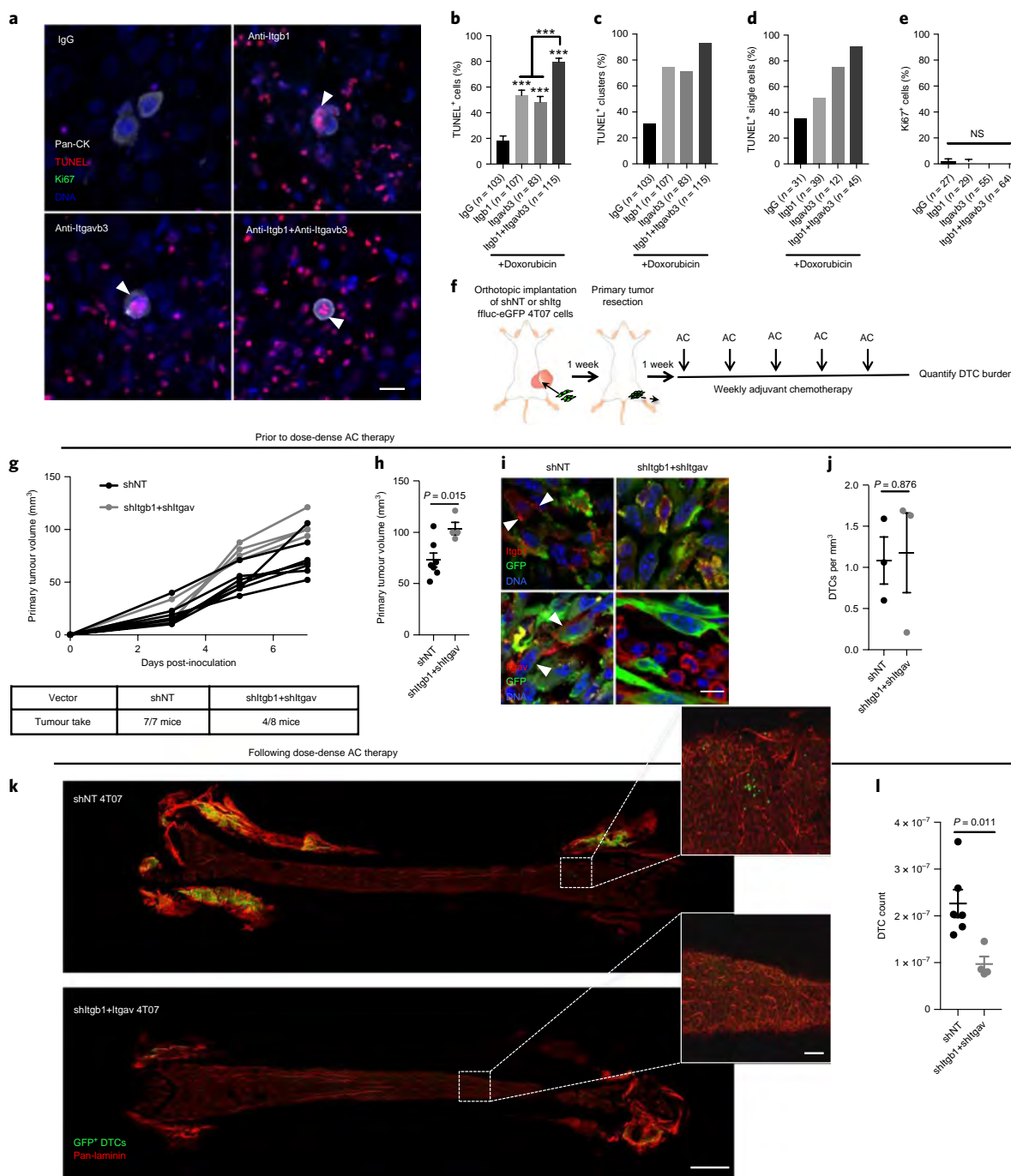


Fig. 6 | Targeting integrin β_1 and integrin α_3 sensitizes BM DTCs to chemotherapy. **a**, TUNEL-stained T4-2 DTCs on BM MVNs following treatment with integrin β_1 and/or integrin α_3 function blocking antibodies and 2,500 nM doxorubicin. White arrowheads indicate apoptotic DTCs. Scale bar, 20 μ m.

b-d, Percentage of TUNEL⁺ DTCs (from predominantly single cells and clusters of 2-4 cells) (**b**), DTC clusters with at least one TUNEL⁺ DTC (**c**) and TUNEL⁺ single cells (**d**). *** $P < 0.0001$ comparing primed conditions to isotype control, or comparing dual-priming to single agent priming, by one-way ANOVA and Tukey's multiple comparison test. **e**, Percentage of Ki67⁺ DTCs after priming. NS, no significance by one-way ANOVA and Tukey's multiple comparison test. **f**, Schematic of experiment to test the combined effect of blocking integrin β_1 and integrin α_3 on DTC survival in response to chemotherapy in vivo.

g, Kinetics of primary tumour growth and take rates for shNT and shltgb1+ltgav 4T07 cells. **h**, Average primary tumour volume of shNT ($n = 7$ animals) and shltgb1+ltgav ($n = 4$ animals) cohorts at resection. * $P = 0.015$ by unpaired, two-tailed t -test. **i**, Representative images of $n = 3$ biologically independent shNT and shltgb1+ltgav 4T07 primary tumours, stained for activated integrin β_1 (top row) and integrin α_3 (bottom row). White arrowheads indicate integrin expression on GFP⁺ tumour cells. Scale bar, 10 μ m. **j**, DTCs per mm³ of BM in an untreated cohort of mice ($n = 3$ femurs from 3 distinct animals), normalized to the primary tumour volume. P value calculated using unpaired, two-tailed t -test. **k**, Representative images of whole-mounted femurs derived from animals treated with dose-dense AC. Scale bar, 1 mm, inset, 100 μ m. **l**, DTCs per femur, normalized to the total area of BM analysed and primary tumour volume. $n = 7$ femurs from 7 different animals were analysed for the shNT condition, $n = 4$ femurs from 4 different animals were analysed for the shltgb1+shltgav condition. P value calculated using unpaired, two-tailed t -test. For TUNEL and Ki67 analyses, the number of cells (predominantly single cells and clusters of 2-4 cells) analysed per condition across $n = 3$ independent experiments is stated within each panel. For **b**, **e**, **h**, **j** and **l**, the centre line represents the mean and the error bars the s.e.m. Source data are provided in Supplementary Tables 1 and 2.

To ensure that this response was specific to the DTC compartment, we used short hairpin RNA (shRNA) to target integrin β_1 (*ITGB1*) in T4-2 cells; this achieved a robust 76% knockdown of integrin β_1 protein (Supplementary Fig. 5a,b). The number of DTCs or DTC clusters present after 12 days of co-culture was unchanged between shITGB1 and non-targeting (NT) control (Supplementary Fig. 5c,d), suggesting that depletion of integrin β_1 does not compromise DTC survival on its own. However, integrin β_1 knockdown substantially reduced DTC proliferation (Supplementary Fig. 5c,e). Following treatment with doxorubicin, the DTC burden was further compromised in the shITGB1 condition (Supplementary Fig. 5g), and the percentage of DTCs positive for TdT-mediated dUTP nickend labelling (TUNEL) increased drastically (Supplementary Fig. 5f,h–j). This level was on par with levels of TUNEL achieved with function blocking antibody (Fig. 4f–h). These results confirm that targeting DTC integrin β_1 compromises survival, but only after application of doxorubicin. These data also lend support to the concept presented in Fig. 3 that the chemotherapeutic response of perivascular DTCs is not linked to proliferation state.

Integrin $\alpha_v\beta_3$ has a restricted binding repertoire, which narrowed considerably when we examined transcriptomic (Fig. 4c) and proteomic data (Fig. 4d) for integrin $\alpha_v\beta_3$ ligands expressed abundantly in MVNs. Staining BM for von Willebrand Factor (VWF), osteopontin (SPP1) and tenascin C (TNC) revealed that only VWF was expressed on the basal surface of BM microvascular endothelium (Fig. 5a), consistent with previous reports^{44–46}. To determine whether endothelial VWF protects breast tumour cells from chemotherapy, a loss-of-function approach was employed. We identified two shRNA clones that knocked down endothelial cell expression of VWF by 48% and 87% (Fig. 5b,c). Using immunofluorescence, we also confirmed that knockdown was sustained over the 27-day course of our experiments (Fig. 5d). Loss of VWF did not affect breast tumour cell survival (Fig. 5e) or outgrowth (Fig. 5f) in the absence of chemotherapy. However, when depletion of endothelial VWF was combined with doxorubicin, up to 70% of single T4-2 cells underwent apoptosis in a manner that correlated with the level of VWF knockdown (Fig. 5g–i). These levels nearly mirrored those obtained with an integrin $\alpha_v\beta_3$ function blocking antibody, suggesting that integrin $\alpha_v\beta_3$ protects DTCs from chemotherapy through signalling triggered by endothelial VWF.

The potent effect of inhibiting the integrin α_4 and β_1 subunits on breast tumour cell survival (Fig. 4f–i) suggested that an endothelial ligand for DTC, integrin $\alpha_4\beta_1$, mediates chemotherapeutic resistance. Vascular cell adhesion molecule 1 (VCAM1)—an integrin $\alpha_4\beta_1$ ligand shown previously to mediate chemoresistance of leukaemia cells⁴⁷—was enriched in BM MVNs (Fig. 4c) and expressed by BM endothelium (Fig. 5a). Therefore, we used a well-characterized antibody that blocks adhesion to VCAM1⁴⁸ to assess whether endothelial VCAM1 protects DTCs from doxorubicin. Consistent with our observations with VWF-depleted endothelium, inhibiting DTC binding to VCAM1 in the absence of doxorubicin did not alter tumour cell survival or proliferation (Fig. 5j,k). However, following doxorubicin administration, a near doubling of TUNEL⁺ cells was observed overall (Fig. 5l), driven primarily by substantial induction of apoptosis in single breast tumour cells (Fig. 5m,n). These levels of apoptosis induction did not fully approach those obtained by blocking integrin α_4 adhesion, suggesting that VCAM1 is one of multiple endothelial-derived integrin $\alpha_4\beta_1$ ligands that confer chemotherapeutic resistance to DTCs.

Blocking integrin-mediated signalling synergizes with chemotherapy to deplete DTCs from BM and prevent metastasis. Given our goal of eradicating DTCs from BM, we sought to determine whether combined inhibition of integrin β_1 and integrin $\alpha_v\beta_3$ would result in an additive effect. Combined treatment with function blocking antibodies targeting integrins β_1 and $\alpha_v\beta_3$ led to at least

one TUNEL⁺ tumour cell in 93% of all DTCs and clusters analysed. Sensitization of 79.6% of DTCs overall (compared with 48.3–53.6% with either antibody on its own) was also observed. Moreover, sensitization of 91% of all single DTCs to doxorubicin (compared with 35.5% for IgG-primed BM MVNs, 51.3% for MVNs primed with antibody targeting integrin β_1 , and 75% for MVNs primed with antibody targeting integrin $\alpha_v\beta_3$) was achieved (Fig. 6a–d). Importantly, priming with these integrin inhibitors did not sensitize DTCs to chemotherapy by inducing cell cycle re-entry. That is, treatment with antibodies alone followed by analysis of Ki67 status revealed that both antibodies essentially pushed all DTCs into G₀/early G₁ (Fig. 6e).

These results motivated us to conduct an experiment to determine whether inhibiting the function of DTC integrins β_1 and $\alpha_v\beta_3$ would result in more effective AC-mediated elimination of DTCs in vivo. We used syngeneic, immunocompetent mice tolerized to ffluc-eGFP⁴⁹ for this experiment. Note that owing to the lack of suitable function blocking antibodies targeting murine integrin $\alpha_v\beta_3$, we employed shRNA-mediated knockdown of integrin α_v (*Itgav*) and integrin β_1 (*Itgb1*). Ffluc-eGFP 4T07 cells incorporating either NT shRNA or shRNA targeting *Itgb1* and *Itgav* (resulting in a down-regulation of 81% and 55% at the protein level, respectively) were inoculated in the inguinal fat pads of syngeneic mice (Fig. 6f). Although the take rate of the double knockdown line was diminished (Fig. 6g), tumours that did take grew more rapidly than their NT counterparts (Fig. 6g,h), despite sustained reduction of integrin β_1 and integrin α_v within the primary tumour (Fig. 6i). The number of DTCs harboured in BM did not vary between the two groups in the absence of chemotherapy (Fig. 6j). However, after five rounds of dose-dense AC, an analysis of whole-mounted femurs revealed that inhibition of integrin β_1 and integrin α_v resulted in a 57.2% reduction in DTC burden within BM (Fig. 6k,l; Supplementary Table 2).

Despite this promising result, we were unable to address the critical question of whether successful eradication of BM DTCs prevents metastasis in this or any other immunocompetent model. We believe this is due to persistent immunogenicity of ffluc and eGFP, even in animals engineered to express these xenogens at an embryonic stage. Consequently, we evaluated an immunocompromised model of breast cancer metastasis to bone employing intracardiac delivery of MCF-7 ER⁺ cells that cluster with the luminal A breast cancer subtype⁵⁰. Luminal breast cancers are the most bone metastatic breast cancer subtype⁵¹ and constitute the majority of late breast cancer recurrences⁵². In BM MVNs, inhibition of integrins β_1 and $\alpha_v\beta_3$ sensitized MCF-7 to doxorubicin in an additive fashion (Fig. 7a–c).

Intracardiac delivery of MCF-7 cells in ovariectomized athymic nude mice allowed the study of luminal breast cancer pathogenesis in the background of oestrogen suppression. Female mice were inoculated with 1×10^5 ffluc-eGFP MCF-7 cells 14–16 days after bilateral ovariectomy, primed with antibody 5 days later, then treated weekly with antibody and AC therapy for four cycles (Fig. 7d). Mice were divided into two cohorts: one killed the day after treatment to quantify DTC burden, the other monitored weekly via bioluminescence imaging (BLI) to track metastasis-free survival (Fig. 7d). In contrast to mice primed with isotype control, mice primed with the integrin β_1 inhibitory antibody AIIB2⁵³ or a combination of AIIB2 and the integrin $\alpha_v\beta_3$ inhibitory antibody LM609⁵⁴ exhibited a marked and significant reduction of DTC burden in clearing-enhanced three-dimensional microscopy (Ce3D)-cleared⁵⁵ and whole-mounted lung (Fig. 7e,f), and in whole-mounted femur (Fig. 7g,h). Of note, priming with AIIB2 or with AIIB2 and LM609 with AC treatment led to a 93.9% and a 94.2% reduction, respectively, in DTC burden within femoral BM (Fig. 7h).

Because mice inoculated with MCF-7 eventually experience bone metastasis at one of a number of sites, including the skull, mandible, vertebrae and femur, we could finally address the

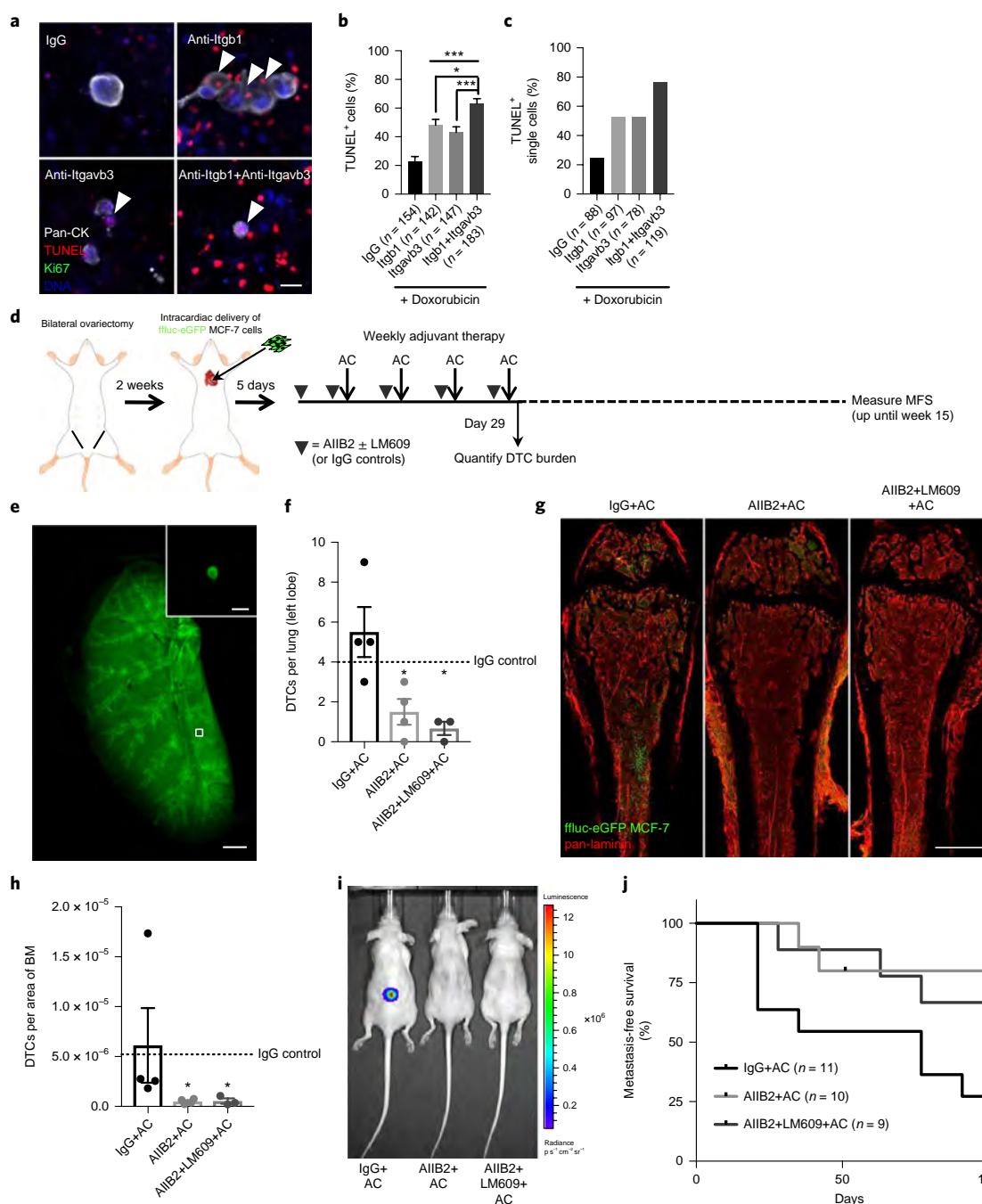


Fig. 7 | Targeting integrin β , sensitizes DTCs to chemotherapy and prevents bone metastasis. **a**, Representative images of TUNEL-stained MCF-7 cells on BM MVNs following priming with integrin β , and/or integrin α ₃ function blocking antibodies and 2,500 nM doxorubicin. White arrowheads indicate apoptotic DTCs. Scale bar, 20 μ m. **b, c**, Percentage of TUNEL⁺ cells from predominantly single cells and clusters of 2-4 cells (**b**) and TUNEL⁺ single cells (**c**). The number of cells or clusters analysed per condition across $n=3$ independent experiments is stated within each panel. *** $P \leq 0.0007$ for IgG primed versus single-agent priming, * $P=0.0149$ for integrin β primed versus dual agent priming, *** $P=0.0004$ for integrin α ₃ primed versus dual agent priming, all by one-way ANOVA and Tukey's post-test. **d**, Schematic of experiment to test the effect of blocking integrin β and integrin α ₃ function on DTC survival and bone metastasis in vivo. **e**, Representative image of the left lobe of a Ce3D⁵⁵-cleared lung, stained for eGFP to quantify lung DTCs. Scale bar, 1 mm. Inset shows a representative DTC. Scale, 10 μ m. **f**, DTCs per lung following treatment (day 29). * $P=0.022$ for AIIB2+AC ($n=4$ lungs from 4 animals) compared with IgG+AC ($n=4$ lungs from 4 animals), $P=0.013$ for AIIB2+LM609+AC ($n=3$ lungs from 3 animals) versus IgG+AC, all by one-way ANOVA and Dunn's post-test. Dashed line represents the mean value for mice treated with IgG only. **g**, Representative images of whole-mounted left femoral heads from animals treated with IgG+AC, AIIB2+AC or AIIB2+LM609+AC. Scale bar, 1 mm. **h**, DTCs per area of BM following treatment (day 29). * $P=0.050$ for AIIB2+AC ($n=4$ femurs from 4 animals) versus IgG+AC ($n=4$ femurs from 4 animals), $P=0.043$ for AIIB2+LM609+AC ($n=3$ femurs from 3 animals) versus IgG+AC, by Kruskal-Wallis test and Dunn's post-test. Dashed line represents the mean value for mice treated with IgG only. **i**, Bioluminescence of mice from each treatment group at week 15. **j**, Kaplan-Meier analysis of metastasis-free survival. * $P=0.039$ by log-rank Mantel-Cox test, $P=0.034$ by Gehan-Breslow-Wilcoxon method. Tick mark represents one censored mouse that died of unknown causes. Cohort sizes are as follows: IgG+AC, 11 animals; AIIB2+AC, 10 animals; AIIB2+LM609+AC, 9 animals. For **b, f, h** and **j** the centre line represents the mean and the error bars the s.e.m. Source data for **b, f, h** and **j** are provided in Supplementary Table 1.

question of whether a reduction of DTC burden equates to metastasis prevention in this model. Over a prescribed 15-week period (Fig. 7d), 73% of mice primed with IgG and treated with AC succumbed to bone metastasis, whereas only 22% of mice primed with AIIB2 and 33% of mice primed with AIIB2 and LM609 relapsed (Fig. 7i,j). Of note, and in agreement with previous work^{56,57}, priming with AIIB2 (or AIIB2 and LM609) did not manifest in overt toxicities affecting body weight (Supplementary Fig. 6a), nor did this regimen alter the density of BM vasculature (Supplementary Fig. 6b). Splenic weight (Supplementary Fig. 6c) was also unchanged over the course of treatment, indicating that gross changes of immune cell content did not occur⁵⁸. This prompted a more thorough examination of viable immune cell populations in the BM of uninoculated, immunocompetent mice. Priming with AIIB2 did not skew AC-driven effects on the number of viable CD45⁺ leukocytes, CD11b⁺ myeloid cells, B220⁺ B cells and CD3⁺ T cells (Supplementary Fig. 6d).

These data confirm that augmenting standard-of-care therapy with an antibody blocking integrin β_1 function results in a drastic reduction in DTC burden and prevention of bone metastasis—all without enhancing chemotherapy-associated toxicity. These data also illustrate the predictive power of organotypic MVNs to accurately reveal the biology and vulnerabilities of disseminated breast tumour cells.

Discussion

Here, we present data showing that the BM MVN protects disseminated breast tumour cells from chemotherapy in a cell cycle-independent fashion. We show that integrin-mediated interactions between DTCs and molecules within the MVN, including VWF and VCAM1, protect DTCs from chemotherapy. Disrupting these interactions sensitizes DTCs to chemotherapy and prevents bone metastasis. Importantly, integrin inhibition neither triggers quiescent DTCs to enter the cell cycle nor exacerbates chemotherapy-associated toxicities. Thus, we anticipate that this finding could ultimately inspire modifications to adjuvant therapy that eradicate DTC burden up front and prevent future metastasis.

A key finding of this work is that sensitization to cytotoxic therapy can be achieved in quiescent cells. Inhibiting integrin β_1 and/or integrin $\alpha_v\beta_3$ sustains cell cycle exit and enhances chemotherapeutic response. This finding is reminiscent of prior work in normal and malignant breast epithelial cells demonstrating that protection from apoptosis-inducing agents is achieved not by quiescence induction but by laminin-induced polarity via integrin $\alpha_6\beta_4$ -mediated hemidesmosome formation²¹. The present work provides several lines of evidence to support the hypothesis⁴ that DTC quiescence and chemoresistance are decoupled. Polarity at the level of single DTCs may be a crucial discriminator.

Translating our findings from organotypic culture to preclinical models led to one surprise. Inhibition of integrin β_1 and integrin $\alpha_v\beta_3$ behaved additively in organotypic culture. However, inhibition of integrin β_1 alone was sufficient to sensitize the vast majority of BM DTCs to AC therapy and to prevent bone metastasis of MCF-7 cells in immunocompromised mice. This result suggests that compromising integrin β_1 function is particularly detrimental to metastasis-initiating DTCs, and emphasizes the need to complement tractable culture models with animal models that allow measurement of metastasis-free survival as a preclinical endpoint.

Despite the marked improvement in metastasis prevention gained from coupling integrin β_1 inhibition with adjuvant therapy, 22% of mice still succumbed to bone metastases. This indicates that some metastasis-initiating cells are left behind despite targeting integrin β_1 . One variable we have not accounted for here is evolution of the DTC microenvironment in response to chemotherapy. Chemotherapy-induced DNA damage of even quiescent

cells causes an array of factors to be secreted, including drivers of chemotherapeutic resistance^{59,60}. Characterizing the chemotherapy-induced secretome of BM vascular endothelium may reveal factors that further enhance DTC survival. We are currently working towards cataloguing this secretome, and postulate that blocking molecules that stimulate parallel (rather than convergent) survival signalling pathways will enhance the elimination of metastasis-initiating DTCs.

Our work provides critical insight about how therapeutic resistance of BM DTCs can be overcome. However, we cannot conclude definitively that elimination of DTCs from BM reflects DTC eradication and metastasis prevention at the systemic level. Addressing this point will determine whether therapies that diminish BM DTC burden prevent metastasis in other cancers, including other breast cancer subtypes, that are more prone to relapse outside the bone. For now, we can conclude that adjuvant chemotherapy can be modified to target the PVN, resulting in depletion of the BM DTC reservoir and prevention of bone metastasis.

Online content

Any methods, additional references, Nature Research reporting summaries, source data, statements of data availability and associated accession codes are available at <https://doi.org/10.1038/s41556-018-0267-0>.

Received: 20 April 2018; Accepted: 14 December 2018;

Published online: 21 January 2019

References

- Karrison, T. G., Ferguson, D. J. & Meier, P. Dormancy of mammary carcinoma after mastectomy. *J. Natl Cancer Inst.* **91**, 80–85 (1999).
- Pan, H. et al. 20-Year risks of breast-cancer recurrence after stopping endocrine therapy at 5 years. *N. Engl. J. Med.* **377**, 1836–1846 (2017).
- Braun, S. et al. Lack of effect of adjuvant chemotherapy on the elimination of single dormant tumor cells in bone marrow of high-risk breast cancer patients. *J. Clin. Oncol.* **18**, 80–86 (2000).
- Ghajar, C. M. Metastasis prevention by targeting the dormant niche. *Nat. Rev. Cancer* **15**, 238–247 (2015).
- Janni, W. et al. Persistence of disseminated tumor cells in the bone marrow of breast cancer patients predicts increased risk for relapse—a European pooled analysis. *Clin. Cancer Res.* **17**, 2967–2976 (2011).
- Sosa, M. S., Bragado, P. & Aguirre-Ghisso, J. A. Mechanisms of disseminated cancer cell dormancy: an awakening field. *Nat. Rev. Cancer* **14**, 611–622 (2014).
- Klein, C. A. Parallel progression of primary tumours and metastases. *Nat. Rev. Cancer* **9**, 302–312 (2009).
- Naume, B. et al. Clinical outcome with correlation to disseminated tumor cell (DTC) status after DTC-guided secondary adjuvant treatment with docetaxel in early breast cancer. *J. Clin. Oncol.* **32**, 3848–3857 (2014).
- Gradishar, W. J. et al. NCCN guidelines insights: breast cancer, version 1.2017. *J. Natl Compr. Canc. Netw.* **15**, 433–451 (2017).
- Jatoi, I. et al. Time-varying effects of breast cancer adjuvant systemic therapy. *J. Natl Cancer Inst.* **108**, djv304 (2016).
- Thurm, H. et al. Rare expression of epithelial cell adhesion molecule on residual micrometastatic breast cancer cells after adjuvant chemotherapy. *Clin. Cancer Res.* **9**, 2598–2604 (2003).
- Mansi, J. L. et al. Bone marrow micrometastases in primary breast cancer: prognostic significance after 6 years' follow-up. *Eur. J. Cancer* **27**, 1552–1555 (1991).
- Braun, S. et al. A pooled analysis of bone marrow micrometastasis in breast cancer. *N. Engl. J. Med.* **353**, 793–802 (2005).
- Naumov, G. N. et al. Ineffectiveness of doxorubicin treatment on solitary dormant mammary carcinoma cells or late-developing metastases. *Breast Cancer Res. Treat.* **82**, 199–206 (2003).
- Pantel, K. et al. Differential expression of proliferation-associated molecules in individual micrometastatic carcinoma cells. *J. Natl Cancer Inst.* **85**, 1419–1424 (1993).
- Boyerinas, B. et al. Adhesion to osteopontin in the bone marrow niche regulates lymphoblastic leukemia cell dormancy. *Blood* **121**, 4821–4831 (2013).
- Cao, Z. et al. Angiocrine factors deployed by tumor vascular niche induce B cell lymphoma invasiveness and chemoresistance. *Cancer Cell* **25**, 350–365 (2014).

18. Cao, Z. et al. Molecular checkpoint decisions made by subverted vascular niche transform indolent tumor cells into chemoresistant cancer stem cells. *Cancer Cell* **31**, 110–126 (2017).
19. Damiano, J. S., Cress, A. E., Hazlehurst, L. A., Shtil, A. A. & Dalton, W. S. Cell adhesion mediated drug resistance (CAM-DR): role of integrins and resistance to apoptosis in human myeloma cell lines. *Blood* **93**, 1658–1667 (1999).
20. Sun, Y. et al. Treatment-induced damage to the tumor microenvironment promotes prostate cancer therapy resistance through WNT16B. *Nat. Med.* **18**, 1359–1368 (2012).
21. Weaver, V. M. et al. Beta4 integrin-dependent formation of polarized three-dimensional architecture confers resistance to apoptosis in normal and malignant mammary epithelium. *Cancer Cell* **2**, 205–216 (2002).
22. Hambarzumyan, D. et al. PI3K pathway regulates survival of cancer stem cells residing in the perivascular niche following radiation in medulloblastoma in vivo. *Genes Dev.* **22**, 436–448 (2008).
23. Ghajar, C. M. et al. The perivascular niche regulates breast tumour dormancy. *Nat. Cell Biol.* **15**, 807–817 (2013).
24. Acharyya, S. et al. A CXCL1 paracrine network links cancer chemoresistance and metastasis. *Cell* **150**, 165–178 (2012).
25. Trumpp, A., Essers, M. & Wilson, A. Awakening dormant haematopoietic stem cells. *Nat. Rev. Immunol.* **10**, 201–209 (2010).
26. Winkler, I. G. et al. Vascular niche E-selectin regulates hematopoietic stem cell dormancy, self renewal and chemoresistance. *Nat. Med.* **18**, 1651–1657 (2012).
27. Calvi, L. M. et al. Osteoblastic cells regulate the haematopoietic stem cell niche. *Nature* **425**, 841–846 (2003).
28. Bruns, I. et al. Megakaryocytes regulate hematopoietic stem cell quiescence through CXCL4 secretion. *Nat. Med.* **20**, 1315–1320 (2014).
29. Butler, J. M. et al. Endothelial cells are essential for the self-renewal and repopulation of Notch-dependent hematopoietic stem cells. *Cell Stem Cell* **6**, 251–264 (2010).
30. Kobayashi, H. et al. Angiocrine factors from Akt-activated endothelial cells balance self-renewal and differentiation of haematopoietic stem cells. *Nat. Cell Biol.* **12**, 1046–1056 (2010).
31. Ding, L., Saunders, T. L., Enikolopov, G. & Morrison, S. J. Endothelial and perivascular cells maintain haematopoietic stem cells. *Nature* **481**, 457–462 (2012).
32. Kiel, M. J. et al. SLAM family receptors distinguish hematopoietic stem and progenitor cells and reveal endothelial niches for stem cells. *Cell* **121**, 1109–1121 (2005).
33. Chen, J. Y. et al. Hoxb5 marks long-term haematopoietic stem cells and reveals a homogenous perivascular niche. *Nature* **530**, 223–227 (2016).
34. Butler, J. M., Kobayashi, H. & Rafii, S. Instructive role of the vascular niche in promoting tumour growth and tissue repair by angiocrine factors. *Nat. Rev. Cancer* **10**, 138–146 (2010).
35. Pantel, K., Braun, S., Passlick, B. & Schlimok, G. Minimal residual epithelial cancer: diagnostic approaches and prognostic relevance. *Prog. Histochem. Cytochem.* **30**, 1–60 (1996).
36. Schmidt-Kittler, O. et al. From latent disseminated cells to overt metastasis: genetic analysis of systemic breast cancer progression. *Proc. Natl Acad. Sci. USA* **100**, 7737–7742 (2003).
37. Gradishar, W. J. et al. Breast cancer version 3.2014. *J. Natl Compr. Canc. Netw.* **12**, 542–590 (2014).
38. Xia, W. et al. Anti-tumor activity of GW572016: a dual tyrosine kinase inhibitor blocks EGF activation of EGFR/erbB2 and downstream Erk1/2 and AKT pathways. *Oncogene* **21**, 6255–6263 (2002).
39. Oki, T. et al. A novel cell-cycle-indicator, mVenus-p27K⁻, identifies quiescent cells and visualizes G0-G1 transition. *Sci. Rep.* **4**, 4012 (2014).
40. Bosch, M. & Franklin-Tong, V. E. Temporal and spatial activation of caspase-like enzymes induced by self-incompatibility in Papaver pollen. *Proc. Natl Acad. Sci. USA* **104**, 18327–18332 (2007).
41. Hirata, E. et al. Intravital imaging reveals how BRAF inhibition generates drug-tolerant microenvironments with high integrin beta1/FAK signaling. *Cancer Cell* **27**, 574–588 (2015).
42. Seguin, L. et al. An integrin beta(3)-KRAS-RalB complex drives tumour stemness and resistance to EGFR inhibition. *Nat. Cell Biol.* **16**, 457–468 (2014).
43. Woelfle, U. et al. Bi-specific immunomagnetic enrichment of micrometastatic tumour cell clusters from bone marrow of cancer patients. *J. Immunol. Methods* **300**, 136–145 (2005).
44. Kusumbe, A. P., Ramasamy, S. K., Starsichova, A. & Adams, R. H. Sample preparation for high-resolution 3D confocal imaging of mouse skeletal tissue. *Nat. Protoc.* **10**, 1904–1914 (2015).
45. Lopes da Silva, M. & Cutler, D. F. von Willebrand factor multimerization and the polarity of secretory pathways in endothelial cells. *Blood* **128**, 277–285 (2016).
46. Nakamura-Ishizu, A. et al. Extracellular matrix protein tenascin-C is required in the bone marrow microenvironment primed for hematopoietic regeneration. *Blood* **119**, 5429–5437 (2012).
47. Weekes, C. D., Kuszynski, C. A. & Sharp, J. G. VLA-4 mediated adhesion to bone marrow stromal cells confers chemoresistance to adherent lymphoma cells. *Leuk. Lymphoma* **40**, 631–645 (2001).
48. Dittel, B. N., McCarthy, J. B., Wayner, E. A. & LeBien, T. W. Regulation of human B-cell precursor adhesion to bone marrow stromal cells by cytokines that exert opposing effects on the expression of vascular cell adhesion molecule-1 (VCAM-1). *Blood* **81**, 2272–2282 (1993).
49. Day, C. P. et al. "Glowing head" mice: a genetic tool enabling reliable preclinical image-based evaluation of cancers in immunocompetent allografts. *PLoS ONE* **9**, e109956 (2014).
50. Holliday, D. L. & Speirs, V. Choosing the right cell line for breast cancer research. *Breast Cancer Res.* **13**, 215 (2011).
51. Harrell, J. C. et al. Genomic analysis identifies unique signatures predictive of brain, lung, and liver relapse. *Breast Cancer Res. Treat.* **132**, 523–535 (2012).
52. Copson, E. et al. Prospective observational study of breast cancer treatment outcomes for UK women aged 18–40 years at diagnosis: the POSH study. *J. Natl Cancer Inst.* **105**, 978–988 (2013).
53. Hall, D. E. et al. The alpha 1/beta 1 and alpha 6/beta 1 integrin heterodimers mediate cell attachment to distinct sites on laminin. *J. Cell Biol.* **110**, 2175–2184 (1990).
54. Cheresch, D. A. Human endothelial cells synthesize and express an Arg-Gly-Asp-directed adhesion receptor involved in attachment to fibrinogen and von Willebrand factor. *Proc. Natl Acad. Sci. USA* **84**, 6471–6475 (1987).
55. Li, W., Germain, R. N. & Gerner, M. Y. Multiplex, quantitative cellular analysis in large tissue volumes with clearing-enhanced 3D microscopy (Ce3D). *Proc. Natl Acad. Sci. USA* **114**, E7321–E7330 (2017).
56. Park, C. C. et al. Beta1 integrin inhibitory antibody induces apoptosis of breast cancer cells, inhibits growth, and distinguishes malignant from normal phenotype in three dimensional cultures and in vivo. *Cancer Res.* **66**, 1526–1535 (2006).
57. Brooks, P. C. et al. Antiintegrin alpha v beta 3 blocks human breast cancer growth and angiogenesis in human skin. *J. Clin. Invest.* **96**, 1815–1822 (1995).
58. Hawkins, E. D. et al. Regulation of asymmetric cell division and polarity by Scribble is not required for humoral immunity. *Nat. Commun.* **4**, 1801 (2013).
59. Gilbert, L. A. & Hemann, M. T. DNA damage-mediated induction of a chemoresistant niche. *Cell* **143**, 355–366 (2010).
60. Gomez-Sarosi, L., Sun, Y., Coleman, I., Bianchi-Frias, D. & Nelson, P. S. DNA damage induces a secretory program in the quiescent TME that fosters adverse cancer phenotypes. *Mol. Cancer Res.* **15**, 842–851 (2017).

Acknowledgements

The authors thank the following people: G. Merlino and C.-P. Day for providing C.FVB-Tg(GNhrh-luc/EGFP)L8Mrln/Lmwj mice; A. Putnam for providing human umbilical vein endothelial cells; S. Beronja for providing murine targeted shRNA constructs; P. Paddison for providing the mVenus-p27K⁻ vector; C. Morse for instruction on bilateral ovariectomy; S. Hingorani for in-depth discussions about preclinical trial design; and P. Lampe for instruction regarding antibody purification. They are also thankful to S. Beronja for his critical feedback on this work. This study was catalysed by start-up funds provided by the Fred Hutchinson Cancer Research Center and a grant from the Cuyamaca Foundation (to C.M.G.), and supported to its completion by an Era of Hope Award from the Department of Defense (DoD) Breast Cancer Research Program (BCRP; W841XWH-15-1-0201 to C.M.G. and K.C.H.), a grant from the Breast Cancer Research Foundation (IIDRP-17-001 to C.M.G.), a grant from the National Breast Cancer Coalition's Artemis Project for Metastasis Prevention, a Physical Sciences Oncology Project Grant from the NIH/NCI (U54CA193461-01 to C.M.G.), and by the Comparative Medicine, Antibody Technology, Experimental Histopathology and Genomics Shared Resources of the Fred Hutchinson/University of Washington Cancer Consortium (P30 CA015704). P.S.N.'s laboratory is supported by the Prostate Cancer Foundation and NIH/NCI grants P50CA097186, U54CA224079 and R01CA165573, and by the DoD awards PC170431 and PC160662. K.C.H.'s laboratory is also supported by a grant from the NIH/NCI (R33CA183685). A.D. is supported by a fellowship from the Terri Brodeur Breast Cancer Foundation, C.A.G. is supported by a postdoctoral fellowship from the Susan G. Komen Foundation, J.D. is supported by a Postdoctoral Breakthrough award by the DoD's BCRP, A.R.L. was supported by a Cardiovascular Pathology Training Grant from the NIH (5T32HL007213-38) and is currently supported by a fellowship from the NIH/NCI (1F31CA228424-01), and S.B.C. is supported by a Cellular and Molecular Biology Training Grant from the NIH (T32GM007270).

Author contributions

P.C., A.D., C.A.G., J.K., R.E.S., E.T.G., J.D., E.M.S., A.R.L. and S.B.C. performed experiments and analysed data. I.M.C. and P.S.N. conducted all procedures related to RNA sequencing, and analysed and interpreted resulting data. A.B. and K.C.H. conducted all ECM-targeted MS, and analysed and interpreted the resulting data. D.A.C. provided critical reagents. D.A.C., P.S.N. and K.C.H. provided scientific insight. C.M.G. conceived the study, conducted experiments, analysed and interpreted data, and wrote the manuscript. All authors read and provided feedback on the manuscript.

Competing interests

The authors declare no competing interests.

Additional information

Supplementary information is available for this paper at <https://doi.org/10.1038/s41556-018-0267-0>.

Reprints and permissions information is available at www.nature.com/reprints.

Correspondence and requests for materials should be addressed to C.M.G.

Publisher's note: Springer Nature remains neutral with regard to jurisdictional claims in published maps and institutional affiliations.

© The Author(s), under exclusive licence to Springer Nature Limited 2019

Methods

Animal studies. All animal work was performed in accordance with Institutional Animal Care and Use Committee (specifically, Fred Hutchinson Cancer Research Center protocol numbers 50865 and 50928) and American Association for Laboratory Animal Science guidelines and ethical regulations.

Modelling spontaneous dissemination and chemoresistance in immunocompetent mice. To quantify the location of DTCs following spontaneous dissemination from orthotopic tumours, 1×10^6 fluc-eGFP 4T07 cells⁶¹ (Karmonos Cancer Institute, Wayne State University) were injected into the inguinal mammary gland of 6–8-week-old female C.FVB-Tg(GNrh-luc/EGFP)L8Mrln/Lmw] (also known as “Glowing Head” (GH))⁴⁹ Balb/c mice in 30 μ l of a 1:1 solution of laminin-rich ECM (LrECM; growth factor-reduced Cultrex, Trevigen):PBS. Tumours were resected at a final volume of ~ 250 mm³ ~ 2.5 weeks later and fixed in a solution of 1.6% paraformaldehyde (PFA), 30% sucrose and PBS overnight (4 °C). Samples were equilibrated in Optimal Cutting Temperature (OCT; Fisher Scientific) embedding compound and 30% sucrose in PBS at 1:1 ratio for 2 h (4 °C) and embedded in OCT compound. BLI was performed on a IVIS Spectrum (Perkin Elmer) 1 week after resection following the intraperitoneal delivery of 100 μ l D-Luciferin (10 mg ml⁻¹, BioVision) to confirm successful resection. Any mice with residual BLI signals were excluded from future study.

To mimic dose-dense chemotherapy in human patients, mice were treated 1 week post-resection with five cycles of weekly administration of Adriamycin (2 mg per kg) and cyclophosphamide (60 mg per kg), paclitaxel (20 mg per kg) or vehicle control²⁴. Chemotherapeutics were purchased from SelleckChem. BLI was performed once more after the cessation of therapy to ensure that relapse at the primary site had not occurred.

Animals were killed 6 weeks post-resection and perfused with ice-cold PBS (25 ml) via the left ventricle (with simultaneous ligation of the inferior vena cava). Femurs and tibia were denuded of connective tissue, fixed in 4% PFA (Electron Microscopy Sciences) in PBS for 2 h at room temperature (RT) and transferred to a solution of 30% sucrose in PBS overnight (4 °C). Samples were equilibrated in a 1:1 solution of OCT:30% sucrose in PBS for 2 h (4 °C) and then embedded flat (that is, with the femoral head and the condyles parallel to the surface) in 24 \times 24 \times 5 mm embedding moulds in OCT compound.

For experiments to study the effect of integrin β_1 and integrin $\alpha_5\beta_1$ on the survival of BM DTCs, NT shRNA or shRNA targeting *Itgb1* and *Itgav* plus fluc-eGFP 4T07 cells were implanted into the inguinal mammary gland of GH-Balb/c mice as described above in a randomized and blinded fashion. Orthotopic tumours were surgically resected after 7 days. One week post-resection, animals underwent BLI to confirm the absence of local recurrence. Mice were subsequently treated with five cycles of AC, and killed 6 weeks post-resection. Femurs were processed as described in the previous paragraph.

Modelling bone metastasis of luminal breast cancer in the setting of oestrogen suppression. Ovariectomy surgery. Female, athymic nude mice (5–6 weeks old; Charles River, Strain 490) were ovariectomized by dual dorsal incisions to expose and dissect the ovaries without damaging the uterine horn. Ovaries were embedded and stained with haematoxylin and eosin (H&E) by the Fred Hutchinson Experimental Histopathology Core. Successful ovariectomies were confirmed for every mouse included in preclinical experiments by a veterinary histopathologist.

Intracardiac injection. Fourteen to 16 days after ovariectomy, anaesthetized mice were positioned in dorsal recumbency on a VisualSonics Vevo 2100 Ultrasound Imaging System to guide injection of 1×10^5 viable fluc-eGFP MCF-7 cells in PBS (100 μ l). MCF-7 cells were triturated after collection by passing five times through a 25-G needle to obtain a single-cell solution, and drawn into a 1-ml syringe mounted with a 22-G needle for injections. The needle height and angle were adjusted on a stereotactic rig, and the needle was guided via ultrasound imaging into the left ventricle. The cell mixture was injected slowly only after visualization of blood refluxing into the syringe. Mice were monitored over the subsequent week via BLI. Mice with residual signals in their heart 1 week post-injection were excluded from further study.

Treatment. Five days post-injection, mice were primed with antibody, then treated weekly (days 7, 14, 21 and 28 post-injection) with antibody and with or without AC. Antibodies consisted of isotype control (250 μ g mouse IgG and 5 mg per kg rat IgG), rat anti-integrin β_1 (A1IB2, 2.7 mg ml⁻¹, 5 mg per kg⁵⁶, Fred Hutchinson Antibody Technology Core, 1.23 EU ml⁻¹), or A1IB2 and mouse anti-integrin $\alpha_5\beta_1$ (LM609, 3.5 mg ml⁻¹, 250 μ g per mouse⁵⁷, UCSD/Cheresh Laboratory, 1.1 EU mg⁻¹). Antibodies were delivered intraperitoneally. Two hours following antibody treatment, AC (2 mg per kg Adriamycin and 60 mg per kg cyclophosphamide) or vehicle control were delivered intraperitoneally. To quantify DTCs remaining after treatment, one cohort of mice was killed on day 29. A second cohort of mice was used to measure metastasis-free survival over a prescribed course of 15 weeks.

Quantification of metastasis-free survival. Mice were imaged weekly via BLI for a total of 15 weeks using the same methodology described above. Mice with a recurrent bioluminescent signal $\geq 10^4$ photons per s per cm² per sr (p s⁻¹ cm⁻² sr⁻¹) that increased over consecutive weeks were considered to have metastases.

BM whole-mounting and immunofluorescence staining. BM whole mounts were generated as described previously⁶². OCT-embedded femurs or tibia were shaved

at 50- μ m intervals on a Leica Cryostat CM3050 S (Leica Microsystems) to expose the BM on one face, reversed, and sectioned to expose the BM on the opposite face. Sliced femurs were thawed from OCT, placed in a 1.7-ml Eppendorf tube, washed twice with PBS and blocked overnight (4 °C) in a solution containing sterile-filtered (0.2 μ m) 20% goat serum with 0.5% Triton X-100 in PBS under constant, gentle agitation by circumferential rotation. Following blocking and permeabilization, bones were incubated for ~ 72 h in block containing a combination of chicken anti-GFP, rabbit anti-pan-laminin, rat anti-VE-cadherin, rabbit anti-VWF, goat anti-osteopontin, rabbit anti-TNC, mouse anti-VCAM1 and/or mouse anti-Ki67-A647 (details regarding these antibodies is provided in Supplementary Table 3). Bones were washed the following day a minimum of six times in PBS before washing overnight at 4 °C. Femurs were then counterstained in blocking solution containing secondary antibodies (Supplementary Table 3) and 4',6-diamidino-2'-phenylindole dihydrochloride (DAPI; 2 μ g ml⁻¹). Femurs were washed again the following day in PBS and finally placed into a solution of PBS with 0.02% sodium azide to preserve the bone before imaging.

For imaging, whole mounts were generated by gently placing femurs in aqueous mounting medium (Fluoromount-G, Southern Biotech) in a 3.5-cm plate containing a No 1.5 coverslip insert (MatTek Corporation, P35G-1.5-20-C) and covering the femur with a 18 \times 18 mm coverslip to press the marrow flush against the imaging window. Tile scans were generated by placing this culture dish on a Zeiss LSM700 and scanning the entire bone using four laser lines and either a 0.17 NA $\times 2.5$ Fluar objective to quantify DTC number or a 0.3 NA $\times 10$ air objective to measure distances between DTCs and specific niches over the entire imageable depth of the marrow (≤ 100 μ m). Images of individual DTCs were acquired using a 0.55 NA $\times 20$ air objective.

Immunofluorescence staining of primary tumour sections. Twenty-five micron sections of fixed and OCT-embedded primary tumours were cut and mounted on Superfrost Plus glass slides. Sections were washed twice with PBS to rehydrate and incubated in 0.5 M glycine in PBS for 1 h at RT. Tissues were simultaneously permeabilized and blocked in a solution containing 0.1% TritonX-100, 5% BSA and 10% goat serum in PBS, before staining with primary antibodies overnight (4 °C). Chicken anti-GFP, mouse anti-integrin β_1 and mouse anti-integrin $\alpha_5\beta_1$ antibodies (Supplementary Table 3) were diluted in a blocking solution of 5% BSA in PBS and applied overnight. The following day, slides were washed repeatedly in PBS and counterstained as described above for femoral whole mounts before imaging using a Zeiss LSM700.

Lung clearing via the Ce3D method and staining of GFP⁺ DTCs. Mice were killed and perfused with ice-cold PBS (25 ml) through the left ventricle. The left lobe of the lung was collected and fixed in 1% PFA in PBS overnight, rocking at 4 °C. Lungs were blocked in 1% normal mouse serum (1.5 ml; MP Biomedicals), 1% BSA (Sigma), 0.3% Triton X-100 (Sigma) in PBS for 8 h at 37 °C in a shaking incubator. Chicken anti-GFP antibody was added to the blocking solution and lungs were incubated in primary antibody solution for 72 h while shaking at 37 °C. Lungs were washed for 24 h in 0.2% Triton X-100 and 0.5% 1-thioglycerol (Sigma) in PBS while shaking at 37 °C. Lungs were submerged in block solution (1.5 ml) containing goat anti-chicken 488 (1:250) and shaken for another 48 h at 37 °C. The wash process was repeated for another 24 h.

After staining, lungs were cleared using Ce3D⁵⁵ solution (40% v/v N-methylacetamide (Sigma), 86% w/v Histodenz (Sigma), 0.1% Triton X-100 and 0.5% 1-thioglycerol in PBS). Lungs were covered and incubated in Ce3D solution (1 ml) on a circumferential rotor for 72 h (RT). Ce3D solution was replaced and lungs were incubated for another 72 h. Cleared lungs were stored in Ce3D solution at RT until imaged. Imaging to quantify DTCs was performed manually in a single blinded fashion on a Zeiss AXIO Zoom.V16 with the aperture set to 65%. Lungs were scanned at 37.5 \times , and structures of interest were confirmed to be cellular in nature at 112 \times . A cleared lung from an uninoculated mouse was used as a control; no DTCs or DTC-like structures were observed in this tissue.

Quantification of primary tumours and DTCs in mice. Mammary tumour measurements. Mammary tumours were measured in vivo and ex vivo using digital calipers to measure the long (L) and short (w) axes of the tumour. Volume (V) was calculated using the equation $V = 0.5 Lw^2$.

DTC localization to specific niches. ZEN Black (Zeiss) was used to load Z-stacked tile scans of femurs and tibia. Distances between GFP⁺ DTCs to the nearest pan-laminin⁺ or VE-cadherin⁺ blood vessel, the nearest megakaryocyte (based on their unique nuclear morphology) and the nearest osteoblast (the interface between BM and bone) were measured manually using this software and tabulated for each identified DTC.

DTC concentration. To gauge the effect of integrin inhibition on DTC burden and response to AC, a custom macro was applied to tile-scanned images to count DTCs in NIH Image J software. BM was traced manually, and the channel containing GFP⁺ DTCs was thresholded to remove all background and create a binary image. DTCs were masked, and “Analyze Particles” was run to count all particles with a size ≥ 50 μ m² and circularity between 0.00 and 1.00. The

obtained value was normalized to the total area of BM imaged. For models involving tumour cell inoculation in the mammary fat pad, this value was further normalized to the volume of the primary tumour measured *ex vivo* after surgical resection to account for any differences in the pool of tumour cells available to disseminate.

Two femurs from two uninoculated GH-Balb/c mice that had undergone the entire staining protocol (including primary antibodies) were used as a reference. These returned a zero value. Initial measurements were confirmed with manual counts to ensure accuracy.

Assessing vessel density in femoral BM. Vessel density within the femoral BM was approximated using the macro for DTC concentration, applied instead to the pan-laminin channel. Here, however, area fraction measurements were conducted within the traced region of the thresholded image to provide a percentage of the area occupied by vasculature within the BM.

Flow-based analysis of immune populations in response to AC therapy with or without AIIB2. Wild-type, 6-week-old female FVB mice were either left untreated or treated over the course of 5 weeks with weekly cycles of IgG, AIIB2, IgG plus AC or AIIB2 plus AC ($n = 3$ mice per group), all at the same doses described above. Mice were killed 1 week post-treatment.

BM from one femur per mouse was isolated at the time of killing by cutting each end of the femur and flushing marrow out with $1 \times$ Hank's balanced salt solution and a 27.5-G insulin syringe. Freshly isolated BM from each mouse was filtered over a 40- μ m filter, treated with ACK lysis buffer for 4 min at RT and then resuspended in PBS with 2% FBS. A total of 1×10^6 BM cells per femur were stained with CD16/32 Fc block (BioLegend, clone 93, 1:100) and a LIVE/DEAD Fixable Aqua Dead Cell Stain kit (Invitrogen, 1:1,000) in PBS for 30 min at RT, followed by washing in PBS with 5% BSA (FACS buffer). Subsequently, samples were stained with antibodies against CD45, CD3, CD11b and B220 (see Supplementary Table 3 for details) all at 1:100 in FACS buffer for 30 min at 4 °C. Samples were again washed in FACS buffer followed by fixation in BD Cytofix (BD Biosciences) for 30 min at 4 °C, washed again in FACS buffer and resuspended in 325 μ l FACS buffer. A volume of 5 μ l of each sample was mixed with AccuCheck counting beads (Invitrogen) at 200,000 beads per ml in a total volume of 200 μ l. All samples were analysed on a BD FACSymphony flow cytometer (BD Biosciences) and analysed using FlowJo v.10 software.

Analyses were gated off of forward by side scatter and single cells. Dead cells were quantified by positive staining for the viability stain. Live cells were further gated off of CD45⁺ and analysed as B220⁺ (B cells) or as CD11b⁺CD3⁺ (myeloid cells) and CD11b⁺CD3⁺ (T cells). Absolute cell counts were quantified by first identifying the total cell number from samples that had AccuCheck beads added to them and dividing the cell events by the number of bead events, multiplied by the concentration of beads, the bead volume/cell volume, and the total volume of the cell sample to be analysed. The total cell number calculated was multiplied by the frequency of single cells and subsequent gated populations of interest, yielding absolute cell counts.

Cell culture and reagents. Freshly isolated human umbilical vein endothelial cells were provided by A. Putnam (University of Michigan) and propagated in fully supplemented EGM-2 growth medium (Lonza). Endothelial cells were processed from umbilical cords obtained by a process considered exempt by the University of Michigan's institutional review board (notice of determination dated 21 August 2014), because the tissue is normally discarded and no identifying information is provided to the researchers who receive the cords. BM-derived human MSCs were obtained commercially (ScienCell) and propagated in low glucose DMEM supplemented with 10% FBS (ThermoFisher). All primary human cells were used in experiments by passage 11. Malignant T4-2 cells were grown in H14 medium on collagen-coated tissue culture flasks⁶³. MCF-7 cells were grown in high glucose DMEM supplemented with 10% FBS.

mCherry-E4orf1 endothelial cells were generated as described previously²³. YFP-T4-2 and YFP-MCF-7 were generated by infection of tumour cells with pLentiCMV/YFP lentivirus followed by selection for 96 h with 1μ g ml⁻¹ puromycin. tdTomato-mVenus-p27K⁻ T4-2 cells were generated by sequential infection with pLentiCMV/tdTomato lentivirus, selection for 96 h with 1μ g ml⁻¹ puromycin, and retrovirally infected with pMXs-IRES-puro/mVenus-p27K⁻ (ref. ⁴⁹) provided by the Paddison Laboratory (Fred Hutchinson Cancer Research Center). As reported previously, this vector encodes a mutant form of p27 that lacks cyclin-dependent kinase inhibitory activity³⁹. Cells were starved to drive them into a quiescent state and then mVenus⁺ cells were sorted by flow cytometry to establish a stable population of tdTomato-mVenus-p27K⁻ T4-2 cells.

Generation of BM MVNs. BM MVNs were generated as previously detailed²³. MSCs were seeded alone at a density of 5×10^4 cells per well in 96-well culture plates or with mCherry-E4 endothelial cells at a 5:1 ratio to generate BM MVNs. Cells were suspended in EGM-2 at a concentration 5×10^4 cells per 100 μ l (stroma only) or 6×10^4 cells per 100 μ l (stroma with endothelial cells). After depositing 100 μ l of cellular suspension per well of a 96-well plate, plates were left undisturbed on a flat surface for 20 min to allow even cell seeding before incubation.

After 10 days, YFP tumour cells were suspended in non-supplemented DMEM/F12 (500 cells per ml). YFP tumour cells were seeded (100 μ l per well) after washing cultures three times with PBS. Cells were allowed to settle for 15–25 min at RT, then a drip of LrECM in DMEM/F12 was slowly added to each well (final concentration of 20%). The LrECM drip condensed for 10–15 min at RT before polymerizing fully at 37 °C. If required, cultures were imaged immediately after seeding on a Zeiss LSM700 confocal microscope using a 0.3 NA $\times 10$ air objective. The objective was centred to each well before acquisition of 512×512 pixel, 6×6 tiles (zoom of 0.7) that captured the near-entirety of each well. Cultures were maintained with media changes every 72 h and imaged again on days 10, 12 and 17 (depending on the experiment).

Treatment with doxorubicin and paclitaxel (Tocris BioScience) were conducted by generating 1,000 \times stocks of each concentration tested and diluting said stock into a minimum of 1 ml of DMEM/F12. Cultures were treated at day -12 and -15 post-seeding of tumour cells. Treatments were controlled by treating with the volumetric equivalent of vehicles (ddH₂O for doxorubicin, dimethylsulfoxide (DMSO) for paclitaxel).

Function blocking experiments were conducted by first priming MVNs at day 10 post-seeding of tumour cells with 100 μ g ml⁻¹ of antibody or the appropriate isotype control in DMEM/F12. Between 46 and 48 h later, medium was removed and 2 \times solutions of antibody were added to the appropriate wells. A 2 \times solution of doxorubicin was added exactly 2 h later. This was repeated at day 15 post-seeding of tumour cells, and cultures were analysed at day 17. Supplementary Table 3 lists all function blocking antibodies (and isotype controls) employed—all purchased or produced in preservative-free format.

Immunofluorescence and TUNEL staining of MVNs. MVNs were fixed in 4% PFA in PBS for 15 min (4 °C), washed three times with ice-cold PBS, and left in 0.5 M glycine in PBS until staining (4 °C) to neutralize any unreacted PFA.

For staining, cultures were washed once with PBS before permeabilization in 0.5% Triton-X100/PBS for 15 min (RT), then washed three more times with PBS. If TUNEL staining was to be conducted, a two-component In Situ Cell Death Detection kit (Roche/Sigma, 12156792910) was thawed and mixed on ice according to manufacturer's instructions. Staining solution (30 μ l) was added to each well before incubation for 1 h (37 °C). Cultures were washed three times in PBS before proceeding with our standard staining protocol.

Cultures were blocked in 5% BSA in PBS (0.2- μ m filtered) for 1 h (RT) before staining in primary antibody diluted in blocking solution overnight with gentle tilt-shaking (4 °C). The following primary antibodies were used: chicken anti-GFP or rabbit anti-pan-cytokeratin (CK; AbCam, ab9377, 1:500) to visualize breast tumour cells; rabbit anti-VWF; and mouse anti-Ki67-A647 (see Supplementary Table 3 for details). Cultures were washed the following morning in PBS (6 washes over 1 h) before staining with secondary antibodies (Supplementary Table 3) diluted in blocking solution for 4–6 h (RT). DAPI (2 μ g ml⁻¹) was added to this solution to visualize nuclei. Finally, cultures were washed extensively with PBS, culminating in an overnight wash before storage in PBS with 0.02% sodium azide. Plates were stored in hydrated glass containers (4 °C) before and after imaging.

Von Kossa and Oil Red O staining of MVNs. BM MVN cultures were generated as described above. Cultures were maintained in EGM-2 for 10 days then fixed with 10% neutral buffered formalin solution (Sigma) at RT for 40 min. Cultures were washed three times with ddH₂O and stored at 4 °C in ddH₂O overnight.

As a positive control, human MSCs were differentiated into adipocytes or osteoblasts using established protocols⁶⁴. Briefly, 1×10^4 MSCs were seeded into 96 well plates in low glucose DMEM containing 10% FBS. The next day, differentiation media were applied. Adipogenic media consisted of 1 μ M dexamethasone (Sigma), 50 μ M indomethacin (Sigma), 500 nM 3-isobutyl-1-methylxanthine (Sigma), 5 μ g ml⁻¹ insulin and 2% FBS in low glucose DMEM. Osteogenic media contained 50 μ M ascorbic acid (Sigma), 10 nM dexamethasone (Sigma), 10 μ M β -glycerophosphate (EMD Millipore) and 2% FBS in low glucose DMEM. MSCs were cultured in differentiation media for 14 (osteogenic) or 21 days (adipogenic), fixed and stained as described below.

Von Kossa staining. All reagents for Von Kossa staining were acquired from American MasterTech Scientific. Formalin-fixed cultures were washed five times with ddH₂O then incubated in 5% sodium nitrate solution and exposed to ultraviolet light at 345 nm for 40 min (RT). Following ultraviolet light exposure, cultures were washed five times in ddH₂O, then incubated in 5% sodium thiosulfate solution for 3 min (RT). Washes in ddH₂O were repeated another five times. Cultures were then incubated in nuclear Fast Red Stain for 5 min (RT), washed five times with ddH₂O and stored at 4 °C in 0.02% sodium azide in ddH₂O. Cultures were imaged on a Zeiss AXIO Zoom.V16 with the aperture set to 37% to acquire maximal depth in the Z-plane, and magnification set to $\times 22$ to capture each well of a 96-well plate in its entirety.

Oil Red O staining. All reagents used in Oil Red O staining were obtained from American MasterTech Scientific. Cultures were washed five times in ddH₂O then incubated in 100% propylene glycol for 2 min (RT). Oil Red O Stain was preheated to 60 °C and added to MVNs immediately following propylene glycol incubation.

Cultures were incubated in warm Oil Red O Stain for 6 min at 60 °C, washed once in 80% propylene glycol/ddH₂O, then washed five times in ddH₂O. Cultures were incubated in modified Mayer's haematoxylin for 1 min (RT), washed again in ddH₂O five times and stored at 4 °C in 0.02% sodium azide in ddH₂O until imaged. Images were acquired on a Nikon Eclipse 80i equipped with a DS-Vi1 high-speed colour camera using a 0.3NA ×10 objective.

Time-lapse acquisition. Time-lapse sequences were acquired using a Zeiss LSM 700 confocal microscope fitted with an environmental chamber to maintain constant temperature (37 °C), humidity and CO₂ (5%). Twelve days after seeding tdTomato-mVenus-p27K⁻ T4-2 cells, cultures were treated with 2,500 nM doxorubicin and 1 μM of caspase-3 and caspase-7 substrate NucView 405 (Biotium)⁴⁰ in non-supplemented DMEM/F12. Images (5 × 5 tiles, 512 × 512 resolution, 8-bit) were acquired at minimal laser power every 20 min for up to 72 h. Six distinct time lapses were acquired for each condition and used to quantify the number of apoptotic events that took place after a single doxorubicin treatment and to record whether these events involved p27⁺ or p27⁻ cells. For the purposes of this analysis, cells that switched p27 status over the course of acquisition were omitted.

Quantification of tumour cell growth, proliferative status and apoptosis in MVNs.

Quantification of normalized tumour cell area fraction. A macro was written using NIH ImageJ software to remove bias from data quantification. For the YFP channel only, day 10, 12 and 17 images (that is, before priming, before chemotherapeutic treatment and post-treatment, respectively) were subjected to the following processes. Contrast was enhanced such that 0.5% of pixels were saturated. The image was then sharpened and a constant threshold was applied to all samples within a given experiment to eliminate variability. The total area fraction of the 6 × 6 tiled image occupied by YFP⁺ cells was then calculated. For each image, the measured area fraction at day 17 was normalized by the corresponding pretreatment value to account for any variations in seeding density or outgrowth from well-to-well. Values obtained for each condition were averaged, and these averages were subsequently normalized to the vehicle-treated control where indicated.

Quantification of TUNEL staining. After TUNEL staining, 12-bit, 2,048 × 2,048 pixel images were acquired on a Zeiss LSM700 using a 0.3NA ×10 air objective. For each pan-cytokeratin⁺ tumour cell or cluster, the number of cells constituting that cluster was counted manually (based on the DAPI signal), and the Ki67 status of each cell in that cluster was tabulated, as was the TUNEL status. Cells were counted as TUNEL⁺ if they had strong (intensity >1 × 10³), non-punctate nuclear signal. Values reported are the percentage of TUNEL⁺ cells for each cluster analysed, averaged for each condition over the total number of cells or clusters analysed.

Quantification of Ki67 positivity. Tumour cells and clusters containing at least one cell with a strong nuclear Ki67 signal were counted manually. The Ki67⁺ fraction was obtained by dividing this number by the total number of YFP⁺ clusters per well.

Whole transcriptome sequencing and analysis. RNA was isolated from two biologically independent MSC and MSC plus endothelial cell cultures that were cultured 12 days in EGM-2 medium using a Qiagen RNeasy Mini Kit according to manufacturer's instructions. RNA concentration, purity and integrity was assessed using a NanoDrop (Thermo Fisher Scientific) and Agilent Bioanalyzer. RNA-seq libraries were constructed from 1 μg of total RNA using an Illumina TruSeq Stranded mRNA LT Sample Prep kit according to the manufacturer's protocol. Barcoded libraries were pooled and sequenced on an Illumina HiSeq 2500, generating 50-bp paired end reads. Sequencing reads were mapped to the hg19 human genome using TopHat v.2.1.0⁶⁵. Gene level abundance was quantified from the filtered alignments in R using the Genomic Alignments Bioconductor package. Differential expression was assessed using transcript abundances as inputs to the edgeR Bioconductor package in R⁶⁶. For edgeR analysis, genes filtered for a minimum expression level of at least 1 count per million reads (CPM) in at least two samples were used to calculate expression differences using an exact test with a negative binomial distribution, applying a significance level of 0.05 with Benjamin-Hochberg false discovery rate (FDR) adjustment. Gene expression results were ranked by their edgeR statistics and used to conduct gene set enrichment analysis (GSEA)⁶⁷ to determine patterns of pathway activity in different groups. We utilized the curated pathways from within the MSigDBv5.1. Over-representation enrichment analysis was performed using the String database⁶⁸ by Fisher's exact test with correction for multiple testing. RNA-seq data have been deposited in the Gene Expression Omnibus (GEO) database under the accession number GSE119153.

shRNA-mediated knockdown of ITGB1, VWF, Itgb1 and Itgav. To target human *ITGB1* and *VWF*, lentivirus was produced from pGIPZ constructs containing non-targeting shRNA, shRNA targeting *ITGB1* or shRNA targeting *VWF*. T4-2 cells or endothelial cells were infected at 5 multiplicity of infection (MOI) and selected in 1 μg ml⁻¹ puromycin. To target murine *Itgb1* and *Itgav*,

lentivirus was produced from pLKO.1 constructs, and fLuc-eGFP 4T07 cells were infected at 5 MOI. Stable knockdowns of both genes were established by sequential infection and subsequent culture in 5 μg ml⁻¹ puromycin. Non-targeting vector was used as a control.

Sequences for all shRNA clones targeting human *ITGB1*, human *VWF*, murine *Itgb1* and murine *Itgav* are provided in Supplementary Table 4.

Western blotting. Tumour cells were lysed in 2% SDS in PBS containing complete protease inhibitor cocktail (Roche) and PhosSTOP phosphatase inhibitor cocktail (Roche). Lysate (20–50 μg) was then separated on a Tris-Glycine 4–20% gel. The human and murine integrin β₁ subunits were probed using a mouse monoclonal antibody (BD Biosciences, 610467, clone 18, 1:500). The murine integrin α₅ subunit was probed using a mouse monoclonal antibody (BD Biosciences, 611012, clone 21, 1:500). Human VWF was probed using a rabbit polyclonal antibody (Dako, A0082, 1:500). Blots were simultaneously probed using a rabbit polyclonal antibody to the nuclear membrane protein lamin A/C as a loading control (Santa Cruz Biotechnology, sc-20681, 1:4,000) and developed on a Li-Cor Odyssey. Densitometry was performed using Odyssey software v.3.0. See Supplementary Table 3 for further details on antibodies.

Analysis of BM stroma and MVNs via liquid chromatography–tandem mass spectrometry (LC–MS/MS). **Reagents.** Reagents were purchased from Sigma-Aldrich unless otherwise noted. Sodium chloride was from Acros Organics (part of Thermo Fisher). Microcentrifuge tubes and other consumables were from Axygen, and RINO Screw Cap Tubes from Next Advance. Formic acid and hydroxylamine (NH₂OH) hydrochloride were from Fluka. Anhydrous potassium carbonate, guanidine hydrochloride, sodium hydroxide and acetonitrile (LC–MS grade) were from Fisher Scientific. Trypsin (sequencing grade, TPCK treated) was from Promega.

Sample preparation. Cultures were established for 12 days in EGM-2, washed extensively with PBS to remove medium, collected and pooled into Eppendorf tubes and flash frozen on dry ice before storage at –80 °C until analysis.

Before analysis, samples were thawed and homogenized in freshly prepared high-salt buffer (50 mM Tris-HCl, 3 M NaCl, 25 mM EDTA, 0.25% w/v CHAPS, pH 7.5) containing 1× protease inhibitor (Halt Protease Inhibitor, Thermo Scientific) at a concentration of 10 mg ml⁻¹. Homogenization took place in a bead beater (Bullet Blender Storm 24, Next Advance, 1-mm glass beads) for 3 min at 4 °C. Samples were then spun for 20 min at 18,000 ×g at 4 °C, and the supernatant removed and stored as Fraction 1. A fresh aliquot of high-salt buffer was added to the remaining pellet at 10 mg ml⁻¹ of the starting weight, vortexed at 4 °C for 15 min and spun for 15 min. The supernatant was removed and stored as Fraction 2. This high-salt extraction was repeated once more to generate Fraction 3, after which freshly prepared guanidine extraction buffer (6 M guanidinium chloride adjusted to pH 9.0 with NaOH) was added at 10 mg ml⁻¹ and vortexed for 1 h at RT. The samples were then spun for 15 min, the supernatant removed and stored as Fraction 4 (sECM). Fractions 1, 2 and 3 (Cellular) were combined and all fractions were stored at –80 °C until further analyses.

Hydroxylamine digestion. The remaining pellets from each tissue, representing insoluble ECM proteins, were digested with hydroxylamine as previously described⁶⁹. Briefly, after chaotrope extraction pellets were treated with freshly prepared hydroxylamine buffer (1 M NH₂OH-HCl, 4.5 M guanidine-HCl, 0.2 M K₂CO₃, pH adjusted to 9.0 with NaOH) at 10 mg ml⁻¹ of the starting tissue weight. The samples were briefly vortexed, then incubated at 45 °C with vortexing for 16 h. Following incubation, the samples were spun for 15 min at 18,000 ×g, the supernatant removed and stored as Fraction 5 (iECM) at –80 °C until further analyses.

Trypsin digestion. For each sample, 200 μl of the Cellular fraction, and 100 μl of the sECM and iECM fractions, were subsequently subjected to reduction, alkylation and enzymatic digestion with trypsin. A filter-aided sample preparation approach, as well as C18 cleanup, was performed as previously described⁷⁰.

LC–MS/MS analysis. Samples were analysed on a Q Exactive HF mass spectrometer (Thermo Fisher Scientific) coupled to an EASY-nanoLC 1000 system through a nanoelectrospray source. The analytical column (100 μm i.d. × 150 mm fused silica capillary) was packed in house with 2.7 μm 80 Å Cortex C18 resin (Phenomenex). The flow rate was adjusted to 400 nl min⁻¹, and peptides were separated over a 120-min linear gradient of 4–28% acetonitrile with 0.1% formic acid. Data acquisition was performed using Xcalibur (v.2.1) software supplied with the instrument. The mass spectrometer was operated in positive ion mode. Full MS scans were acquired in the Orbitrap Mass Analyzer over the 300–2,000 *m/z* range with 60,000 resolution. Automatic gain control (AGC) was set at 1.00E+06 and the 15 most intense peaks from each full scan were fragmented via high collision dissociation with a normalized collision energy of 28. MS2 spectra were acquired in the Orbitrap Mass Analyzer with 15,000 resolution with the AGC set at 1.00E+05. All replicates of each tissue were run sequentially, and pre-digested yeast

alcohol dehydrogenase standard (nanoLCMS Solutions) was run between sample groups to monitor drift in analytical performance.

Database searching and protein identification. MS/MS spectra were extracted from raw data files and converted into .mgf files using Pava (UCSF). Peptide spectral matching was performed with Mascot (v.2.5) against the UniProt mouse database (release 201701). Mass tolerances were ± 10 ppm for parent ions, and ± 0.2 Da for fragment ions. Trypsin specificity was used for cellular and sECM fractions, allowing for one missed cleavage. For the iECM fraction, carboxy-terminal N and trypsin were used, allowing for one missed cleavage. Met oxidation, Pro hydroxylation, protein amino-terminal acetylation and peptide amino-terminal pyroglutamic acid formation were set as variable modifications with Cys carbamidomethylation set as a fixed modification. Scaffold (v.4.4.6, Proteome Software) was used to validate MS/MS-based peptide and protein identifications. Peptide identifications were accepted if they could be established at greater than 95.0% probability as specified by the Mascot scoring algorithm. Protein identifications were accepted if they could be established at greater than 99.0% probability and contained at least two identified unique peptides. Metaboanalyst was used for multivariate analysis of proteomic data.

Statistics and reproducibility. Statistical analyses were conducted using GraphPad Prism 7 software. Data that were distributed normally were compared via unpaired two-tailed *t*-test (if only two conditions were tested) or via one- or two-way analysis of variance (ANOVA; for experiments containing three or more conditions). Post-testing to correct for multiple comparisons was chosen based on whether a decision was made a priori to compare conditions to vehicle (Dunnett's) or to compare all treatment groups with each other (Tukey's). Data that were not distributed normally were tested via Kruskal–Wallis and Dunn's post-test to correct for multiple comparisons. Please refer to figure legends for individual *n* and *P* values and the specific statistical test (or tests) employed. Unless noted otherwise, data are reported such that the centre line represents the mean and error bars represent the s.e.m. Experiments were repeated independently, with similar results obtained.

Reporting Summary. Further information on research design is available in the Nature Research Reporting Summary linked to this article.

Code availability

Codes used in this study (for example, ImageJ macros for image analysis) are freely available from the corresponding author upon reasonable request.

Data availability

RNA-seq data that support the findings of this study have been deposited in the GEO under accession code [GSE119153](https://www.ncbi.nlm.nih.gov/geo/query/acc.cgi?acc=GSE119153). MS data have been deposited in the ProteomeXchange Consortium via the PRIDE partner repository with the dataset identifier [PXD012002](https://www.ebi.ac.uk/pride/archive/projects/PXD012002). Source data for Figs. 1c,f–h, 2b,c,e,g–i,k,m, 3a,b,e,h, 4g,i, 5c,e–g,i–m, 6b,e,h,j,l and 7b,f,h,j, and Supplementary Figs. 1c–e, 3a–l, 4b,c, 5b,d,e,g,h,j and 6a–d have been provided as Supplementary Table 1. All other data supporting the findings of this study are available from the corresponding author upon reasonable request.

References

- Miller, B. E., Miller, F. R., Wilburn, D. J. & Heppner, G. H. Analysis of tumour cell composition in tumours composed of paired mixtures of mammary tumour cell lines. *Br. J. Cancer* **56**, 561–569 (1987).
- Nombela-Arrieta, C. et al. Quantitative imaging of haematopoietic stem and progenitor cell localization and hypoxic status in the bone marrow microenvironment. *Nat. Cell Biol.* **15**, 533–543 (2013).
- Briand, P., Nielsen, K. V., Madsen, M. W. & Petersen, O. W. Trisomy 7p and malignant transformation of human breast epithelial cells following epidermal growth factor withdrawal. *Cancer Res.* **56**, 2039–2044 (1996).
- Tang, Y. et al. MT1-MMP-dependent control of skeletal stem cell commitment via a beta1-integrin/YAP/TAZ signaling axis. *Dev. Cell* **25**, 402–416 (2013).
- Kim, D. et al. TopHat2: accurate alignment of transcriptomes in the presence of insertions, deletions and gene fusions. *Genome Biol.* **14**, R36 (2013).
- Robinson, M. D., McCarthy, D. J. & Smyth, G. K. edgeR: a Bioconductor package for differential expression analysis of digital gene expression data. *Bioinformatics* **26**, 139–140 (2010).
- Subramanian, A. et al. Gene set enrichment analysis: a knowledge-based approach for interpreting genome-wide expression profiles. *Proc. Natl Acad. Sci. USA* **102**, 15545–15550 (2005).
- Szklarczyk, D. et al. The STRING database in 2017: quality-controlled protein–protein association networks, made broadly accessible. *Nucleic Acids Res.* **45**, D362–D368 (2017).
- Barrett, A. S. et al. Hydroxylamine chemical digestion for insoluble extracellular matrix characterization. *J. Proteome Res.* **16**, 4177–4184 (2017).
- Goddard, E. T. et al. Quantitative extracellular matrix proteomics to study mammary and liver tissue microenvironments. *Int. J. Biochem. Cell Biol.* **81**, 223–232 (2016).

Reporting Summary

Nature Research wishes to improve the reproducibility of the work that we publish. This form provides structure for consistency and transparency in reporting. For further information on Nature Research policies, see [Authors & Referees](#) and the [Editorial Policy Checklist](#).

Statistical parameters

When statistical analyses are reported, confirm that the following items are present in the relevant location (e.g. figure legend, table legend, main text, or Methods section).

n/a Confirmed

- The exact sample size (n) for each experimental group/condition, given as a discrete number and unit of measurement
- An indication of whether measurements were taken from distinct samples or whether the same sample was measured repeatedly
- The statistical test(s) used AND whether they are one- or two-sided
Only common tests should be described solely by name; describe more complex techniques in the Methods section.
- A description of all covariates tested
- A description of any assumptions or corrections, such as tests of normality and adjustment for multiple comparisons
- A full description of the statistics including central tendency (e.g. means) or other basic estimates (e.g. regression coefficient) AND variation (e.g. standard deviation) or associated estimates of uncertainty (e.g. confidence intervals)
- For null hypothesis testing, the test statistic (e.g. F , t , r) with confidence intervals, effect sizes, degrees of freedom and P value noted
Give P values as exact values whenever suitable.
- For Bayesian analysis, information on the choice of priors and Markov chain Monte Carlo settings
- For hierarchical and complex designs, identification of the appropriate level for tests and full reporting of outcomes
- Estimates of effect sizes (e.g. Cohen's d , Pearson's r), indicating how they were calculated
- Clearly defined error bars
State explicitly what error bars represent (e.g. SD, SE, CI)

Our web collection on [statistics for biologists](#) may be useful.

Software and code

Policy information about [availability of computer code](#)

Data collection

Whole transcriptome sequencing and analysis. RNA concentration, purity, and integrity was assessed by NanoDrop (Thermo Fisher Scientific Inc) and Agilent Bioanalyzer. RNA-seq libraries were constructed from 1 ug total RNA using the Illumina TruSeq Stranded mRNA LT Sample Prep Kit according to the manufacturer's protocol. Barcoded libraries were pooled and sequenced on the Illumina HiSeq 2500 generating 50 bp paired end reads.

Data analysis

Sequencing reads were mapped to the hg19 human genome using TopHat v2.1.0 (<https://www.ncbi.nlm.nih.gov/pubmed/23618408>). Gene level abundance was quantitated from the filtered alignments in R using the Genomic Alignments Bioconductor package. Differential expression was assessed using transcript abundances as inputs to the edgeR Bioconductor package in R (<https://www.ncbi.nlm.nih.gov/pubmed/19910308>). For edgeR analysis, genes filtered for a minimum expression level of at least 1 count per million reads (CPM) in at least two samples were used to calculate expression differences using an exact test with a negative binomial distribution, applying a significance level of 0.05 with Benjamin-Hochberg false discovery rate (FDR) adjustment.

A custom Image J macro was used for analysis of DTCs/bone marrow area and is available upon request.

For manuscripts utilizing custom algorithms or software that are central to the research but not yet described in published literature, software must be made available to editors/reviewers upon request. We strongly encourage code deposition in a community repository (e.g. GitHub). See the Nature Research [guidelines for submitting code & software](#) for further information.

Data

Policy information about [availability of data](#)

All manuscripts must include a [data availability statement](#). This statement should provide the following information, where applicable:

- Accession codes, unique identifiers, or web links for publicly available datasets
- A list of figures that have associated raw data
- A description of any restrictions on data availability

RNA sequencing data have been deposited in the Gene Expression Omnibus database under the accession number GSE119153.

Mass spectrometry data have been deposited in to the ProteomeXchange Consortium via the PRIDE partner repository with the dataset identifier PXD012002.

Field-specific reporting

Please select the best fit for your research. If you are not sure, read the appropriate sections before making your selection.

Life sciences Behavioural & social sciences Ecological, evolutionary & environmental sciences

For a reference copy of the document with all sections, see nature.com/authors/policies/ReportingSummary-flat.pdf

Life sciences study design

All studies must disclose on these points even when the disclosure is negative.

Sample size	We conducted culture experiments a minimum of three independent times, at minimum in triplicate. The majority of culture experiments were conducted five independent times. We typically analyzed >100 cells from single cells or clusters of mostly 2-4 cells to define the percentage of TUNEL-positive cells. These samples were pooled across three independent experiments.
Data exclusions	Data were not excluded.
Replication	All attempts at replication were successful.
Randomization	Randomization applies principally to the animal experiments presented in Figures 6 and 7. A random number generator with pre-determined even-odd assignments was utilized to assign mice to each experimental group.
Blinding	The individuals conducting animal experiments were blinded during treatment and data analysis. Blinding was not performed for cell culture experiments. With the exception of TUNEL staining, these have automated inputs and outputs that remove bias.

Reporting for specific materials, systems and methods

Materials & experimental systems

n/a	Involved in the study
<input type="checkbox"/>	<input checked="" type="checkbox"/> Unique biological materials
<input type="checkbox"/>	<input checked="" type="checkbox"/> Antibodies
<input type="checkbox"/>	<input checked="" type="checkbox"/> Eukaryotic cell lines
<input checked="" type="checkbox"/>	<input type="checkbox"/> Palaeontology
<input type="checkbox"/>	<input checked="" type="checkbox"/> Animals and other organisms
<input type="checkbox"/>	<input checked="" type="checkbox"/> Human research participants

Methods

n/a	Involved in the study
<input checked="" type="checkbox"/>	<input type="checkbox"/> ChIP-seq
<input type="checkbox"/>	<input checked="" type="checkbox"/> Flow cytometry
<input checked="" type="checkbox"/>	<input type="checkbox"/> MRI-based neuroimaging

Unique biological materials

Policy information about [availability of materials](#)

Obtaining unique materials	This study involved the use of laminin-rich extracellular matrix (lrECM) to overlay co-cultures. The specific type of lrECM employed was Reduced Growth Factor Basement Membrane Matrix (Trevigen, Catalog Number 3433-005-01) Matrigel exhibits substantial lot-to-lot variability. For this study, we used two lots of Cultrex:
----------------------------	---

Lot1: 28337G13

Lot2: 34601M15

Antibodies

Antibodies used	Antibodies used in this study for immunostaining, immunoblotting, flow cytometry and function blocking experiments are detailed in Supplementary Tables 3 and 4.
Validation	GFP antibodies were validated using isotype controls and also by staining mice that were not inoculated with GFP+ cells with the entire staining protocol (including GFP antibody) ensure that staining was null. All other staining antibodies used were chosen due to extensive use in prior publications, and validated independently for specificity by using isotype controls. All integrin blocking antibodies used in our study have been referenced extensively in the literature for target specificity and for blocking adhesion via specific integrin subunits.

Eukaryotic cell lines

Policy information about [cell lines](#)

Cell line source(s)	HMT-3522-T4-2 cells were generously provided by Dr. Mina Bissell. MCF-7 cells were obtained from ATCC. 4T07 cells were purchased directly from the Karmanos Cancer Institute (Wayne State University), where they were derived originally in Dr. Fred Miller's laboratory.
Authentication	T4-2 cells were authenticated routinely by their characteristic 2D and 3D morphologies. MCF-7 cells were authenticated via short tandem repeat (STR) fingerprinting.
Mycoplasma contamination	Cells are mycoplasma tested upon arrival and every 6 months thereafter in the Ghajar Laboratory. No cell that we have maintained, including any of the cell lines or primary cells used in this study, have become contaminated with mycoplasma.
Commonly misidentified lines (See ICLAC register)	No commonly misidentified cell lines were used in this study.

Animals and other organisms

Policy information about [studies involving animals](#); [ARRIVE guidelines](#) recommended for reporting animal research

Laboratory animals	<p>Species: mus musculus Strain: C.FVB-Tg(GNrhr-luc/EGFP)L8Mrln/Lmwj Sex: Female Age: inoculated at 6-8 weeks of age</p> <p>Species: mus musculus Strain: BALB/cAnNCrI Sex: Female Age: inoculated at 6-8 weeks of age</p> <p>Species: mus musculus Strain: Athymic Nude (CrI:NU(NCr)-Foxn1nu) Sex: Female Age: Ovariectomized at 5-6 weeks of age, inoculated via intracardiac injection 14-16 days later.</p>
Wild animals	N/a.
Field-collected samples	N/a.

Human research participants

Policy information about [studies involving human research participants](#)

Population characteristics	Umbilical cords were obtained and processed to isolate human umbilical vein endothelial cells by a process considered exempt by the University of Michigan's institutional review board (notice of determination dated August 21, 2014) because the tissue is normally discarded, and no identifying information is provided to the researchers who receive the cords.
Recruitment	N/a.

Plots

Confirm that:

- The axis labels state the marker and fluorochrome used (e.g. CD4-FITC).
- The axis scales are clearly visible. Include numbers along axes only for bottom left plot of group (a 'group' is an analysis of identical markers).
- All plots are contour plots with outliers or pseudocolor plots.
- A numerical value for number of cells or percentage (with statistics) is provided.

Methodology

Sample preparation

Flow plots are not presented, thus the top 3 boxes are not checked.

Bone marrow from 1 femur/mouse was isolated at the time of euthanasia by cutting each end of the femur and flushing marrow out with 1x HBSS and a 27.5-gauge insulin syringe. Freshly isolated bone marrow from each mouse was filtered over a 40 µm filter, treated with ACK lysis buffer for 4 min at RT, and resuspended in PBS + 2% FBS. 1x10⁶ bone marrow cells/femur were stained with CD16/32 Fc block (BioLegend, clone 93, 1:100) and LIVE/DEAD™ Fixable Aqua Dead Cell Stain Kit (Invitrogen, 1:1000) in PBS for 30 min at RT, followed by washing in PBS + 5% BSA (FACS buffer). Subsequently, samples were stained with antibodies against CD45, CD3, CD11b, and B220 (clones 30-F11, 145-2C11, M1/70, and RA3-6B2, respectively; BioLegend) all at 1:100 in FACS buffer for 30 min at 4 °C. Samples were again washed in FACS buffer followed by fixation in BD Cytofix™ (BD Biosciences) for 30 min at 4 °C, washed again in FACS buffer and resuspended in 325 µl FACS buffer. 5 µl of each sample was mixed with AccuCheck counting beads (Invitrogen) at 200,000 beads/mL in a total volume of 200 µl.

Instrument

BD FACSymphony™ flow cytometer (BD Biosciences)

Software

FlowJo™ v10

Cell population abundance

Absolute cell counts were quantified by first identifying the total cell number from samples that had AccuCheck beads added to them and dividing the cell events by the number of bead events, multiplied by the concentration of beads, the bead volume/cell volume, and the total volume of the cell sample to be analyzed. The total cell number calculated was multiplied by the frequency of single cells and subsequent gated populations of interest, yielding absolute cell counts.

Gating strategy

Analyses were gated off of forward by side scatter and single cells. Dead cells were quantified by positive staining for the viability stain. Live cells were further gated off of CD45+ and analyzed as B220+ (B cells) or as CD11b+CD3- (myeloid cells) and CD11b-CD3+ (T cells).

- Tick this box to confirm that a figure exemplifying the gating strategy is provided in the Supplementary Information.